An investigation of the neutron radiation shielding potential of PEI/H_3BO_3 composite for space missions

Uyen Nguyen

Bachelor's degree Thesis
Material Processing Technology
2020

DEGREE THESIS	
Arcada	
Degree Programme:	Material Processing Technology
Identification number:	22012
Author:	Uyen Nguyen
Title:	An investigation of the neutron radiation shielding potential of PEI/H_3BO_3 composite for space missions.
Supervisors:	Stewart Makkonen-Craig and Erik Brücken
Commissioned by:	

Abstract:

The study of space and its exploration play an important role in the evolution of technologies and the development of human civilization. One of the biggest problems facing the interplanetary spaceflight missions is cosmic neutron radiation. To support these missions, the thesis aims to investigate the neutron shielding potential of new composite (PEI/H_3BO_3) inspired by theoretical studies. Three PEI composites with different H_3BO_3 content (10 wt%, 20 wt% and 30 wt%) were produced using the solvent casting method with N,N-Dimethylformamide (DMF) as the dissolved solvent. In this thesis, the goal was to study and compare the neutron shielding efficiency through the method of pulse-height analysis (PHA) between the three contents of PEI composite. The applied neutron source was an Am-Be source that generates fast non-monoenergetic neutron energy (MeV). In the end, the solvent technique was not successful, as the relative thickness and the theoretical areal density for the composites were not achieved. This led to a non-relative comparison of neutron shielding potential between each content of PEI/H_3BO_3 composite. As the result of the solvent experiment, there were some particles found within the composite supernatant, which were assumed to be H_3BO_3. The UV-Vis spectrophotometer was used to determine the quantity of H_3BO_3 within the solution supernatant that could not react with the precipitated composite. However, the provided data were inaccurate since there were more unidentified impurities than expected. In the PHA, it was recorded that the 30 wt% sample has the highest total neutron count while 20 wt% sample has the lowest, as had been expected after the material production due to the thickness and some trapped solvent. Due to the limited time frame of COVID-19 outbreak, the experiment could not have been repeated many times, causing the lack of confirmation on the result of the neutron count. Although the experiment was not fully accomplished, PEI/H_3BO_3 composite still showed its shielding effectiveness against fast neutron energy in the PHA test. With proper experimental work, the potential of using this combined material for neutron shielding in a space environment may be worthwhile for future space missions.

Keywords:	Polymer composite, polyetherimide, boric acid, solvent casting method, pulse-height analysis, neutron shielding technology, space application.
Number of pages:	63
Language:	English
Date of acceptance:	

CONTENTS

Figures

Tables

LIST OF ABBREVIATIONS

B_2O_3	Boron Trioxide
B_4C	Boron Carbide
Bi_2O_3	Bismuth oxide
BN	Boron Nitride
BPADA	4,4'-Bisphenol A Dianhydride
BPDA	Biphenyl Dianhydride
CERN	European Organization for Nuclear Research
$CHCl_3$	Chloroform
C_5H_5N	Pyridine
DCM	Dichloromethane
DMAc	Dimethylacetamide
DMF	N, N-Dimethylformamide
DMSO	Dimethyl sulfoxide
DPO	Digital Phosphor Oscillator
DSC	Differential Scanning Calorimetry
EPDM	Ethylene Propylene Diene monomer rubber
GCR	Galactic Cosmic Radiation
H_2SO_4	Sulfuric Acid
H_3BO_3	Boric Acid
HDPE	High-density polyethylene
ISS	International Space Station
LEO	Low-Earth Orbit
MCA	Multichannel Analyzer
MSDS	Material Safety Data Sheet
MSL	Mars Science Laboratory
NASA	National Aeronautics and Space Administration
NMP	N-Methyl-2-pyrrolidone
ODA	4,4'-Oxydianiline
PA	Polyamide
PE	Polyethylene
PEI	Polyetherimide
PI	Polyimide
PP	Polypropylene
PPD	P-phenylenediamine
RAD	Radiation Assessment Detector
SEM	Scanning Electron Microscope
TGA	Thermogravimetric analysis
UV-Vis	Ultraviolet-Visible Spectrophotometry
Wt%	Weight percentage

ACKNOWLEDGEMENT

The journey of studying overseas at Arcada University of Applied Sciences has given me numerous valuable memories, knowledge, and skills in the preparation for my future achievement. From the bottom of my heart, I am truly grateful to study in an international environment and to experience a different perspective that I had never encountered before. The time here has strongly motivated me to pursue my goal, which is to contribute my piece of knowledge into the development of space technology.

This thesis reflects myself, where my desire to improve space applications was expressed. The time working with this project was one of the greatest and most enjoyable times of my life. To be honest, it is also the hardest topic that I had ever encountered, and I could not ever overcome it without the support from my beloved ones.

First of all, I wish to express my greatest appreciation to Professor Richard L. Kiefer, for his dedication to a student from the other side of the world. I am extremely thankful for his wise and conscientious advice, which helped me a lot in overcoming the obstacle of producing the polymer composite at the beginning of this thesis. Secondly, I wish to thank my closest friends: Denise Nurmi, Tobias Jansson, Alexander Clark and to my family, who are always willing to support me at any time.

The project would not be possible without the support from SABIC. Therefore, I would like to specifically express my gratefulness to Timo Latvakangas, who had donated one of the main shielding materials for this thesis. His generousity had helped the research greatly in the beginning.

Above all, I wish to pay my sincere regards to my supervisor at the University of Helsinki, Erik Brücken, who has always been enthusiastic and dedicated to delivering me his precious knowledge and experience of neutron measurement. Without his persistent guidance, the goal of this thesis could not be completed. To my thoughtful supervisor at Arcada, Stewart Makkonen-Craig, thank you for all your encouragement, advice, and ideas that you had offered me from the start.

Finally, I wish to send my love to my beloved partner, Tim Gebert, who has always been there for me physically and mentally at the harshest time of my life. I could not have finished this without you.

1 INTRODUCTION

1.1 Background

The journey of exploring and studying the space has been humanity's essential, inseparable and long-term mission for thousands of years. As our great astrophysicist Stephen Hawking (2018, p.165) once addressed:

"Not to leave planet Earth would be like castaways on a desert not trying to escape."

Curiosity and exploration have been humanity's spirit for centuries (Why we explore 2000), which existed to accomplish something greater for the future. Since Columbus discovered the New World in 1492, the future of humanity had changed completely in a positive way, and this effect would be much greater when it comes to the space exploration (Hawking 2018, p.165). The mystery of what is beyond the sky has motivated humanity to explore the new worlds out there, to seek the knowledge and hidden answers in other dimensions, and to overcome the limitation of technologies and the boundary of scientific understanding. Thanks to the study of space, not only advanced technologies can be developed, but also the historical questions about the universe (such as the big bang theory) or scientific knowledge of the solar system, planets, meteorology, asteroid prediction, radiations, etc... can be answered. The journey helps us to determine the role of humanity in the universe, to solve the demanding problems (e.g. climate change) from a different perspective and to look outwards rather than inwards (Hawking 2018, p.166). Interplanetary spaceflight which is an astonishing achievement in history played an important role in this journey. With the interests and the challenges to explore the universe, the further big questions that had been asked for decades can also be answered.

The discovery of cosmic radiation in the early 20th century (Angelis 2013) has greatly influenced scientific study, especially on the evolution of space technology. Since the early 21st century, it has been desired to launch not only unmanned space probes, robotics and satellites into the space environment for deep space exploration, but also spaceships for human discovery and colonization of planets (Logsdon 2019). Radiation is one of the main hazards for space structures and astronauts. For long-term space exploration, shielding technology must be established to minimize radiation exposure. However, this is less of a concern for missions performed in Low-earth orbit (LEO) at altitude of 160 to 2000 km above Earth's surface. Thanks to Earth's atmosphere and magnetosphere, living

species and inanimate objects are protected on the planet and in the LEO zone from most space radiation (Lloyd et al. 2017, p.10). To date, most manned space missions working in space were performed in the LEO environment. For example, the International Space Station (ISS) is where most space explorations are accomplished by astronauts with a distance of 320 to 380 km from the Earth's surface. Moreover, this is also the allowable distance for the artificial satellites to be well-functional for the study of Earth. (Williams, 2017)

The desire for space study is more than exploring within the LEO's environment. Curiosity has motivated humanity to step farther, endeavouring to discover the unknown universe at a further distance. This was proved through the mission Apollo 11 where humanity first landed on the Earth's satellite – the Moon in 1969 (Paine 1969) and achieved the farthest distance in the space exploration's history. The current goal is for numerous interplanetary spaceflights, including the recent announcement of travelling to the Moon again and Mars. That is to say, the proper shielding materials and techniques for different types of radiation are essetial for the mission's preparation. In this thesis, the interest is to study shielding against cosmic-ray neutron radiation for the long-term space missions. Because of its electrically neutral characteristic, neutron radiation can cause higher damage and deeper penetration into matter's structure than primary radiations, making it the most dangerous type.

Heavy metals and their composites are traditionally applied to attenuate the amount of radiation exposure in nuclear and space application. However, using heavy metals as a neutron shield for a long-term space mission might be ineffective, since they create vast amount of secondary particles when encountering primary radiation, causing more damage to engines and humans (Nambiar & Yeow 2012). To avoid these hazards, a composite material which is made of the combination of two or more different components is suggested. The composite is usually preferred as an ideal material since it contains two separate components but still in a fine, homogeneous structure, providing multifunctional benefits (strength, lightweight and cost-effective) than individual materials (Nagavally 2017). In this case, the development of polymer composites has been studied recently for the purpose fo neutron radiation shielding in the space environment. Neutron shielding materials are required to possess a low atomic number with high scattering cross-section, such as hydrogen, carbon or oxygen (McAlister 2016). Some hydrogen-rich polymers

having all three mentioned elements are predicted to have a greater potential of neutron toleration as compared to traditional materials. Hence, polymers are chosen to be the key research of this thesis in neutron shielding. However, applying pure polymers draws two major disadvantages: a weak mechanical strength and continuous damage. The solution is to introduce a potential neutron-capturing compound into the polymer matrix, thus improving polymer strength as well as providing multifunctional material. The study of this composite is assumed to achieve more advantages for the shielding against cosmic-ray neutron as compared with traditional materials.

The main motivation of this thesis is to develop and support human's technologies for space exploration. The project is inspired by the recent announcement of National Aeronautics and Space Administration (NASA), that astronauts will be sent to the Moon on its Lunar South Pole by 2024 (Landau 2019) and there are plans to return to Mars by 2030 (Daines 2017). In the preparation for these missions, radiation protection is one of the major concerns. Therefore, it is important to contribute to the research of polymer composites and their improvement in radiation shielding for interplanetary spaceflight missions. The thesis also wishes to take part in the advancement of radiation shielding technology for artificial machines such as satellites and space probes, which are mainly used for the study of Earth and astronomy. In addition to space exploration, this research aims to contribute the knowledge for the demand for safe neutron-radiation shielding in nuclear technology as well.

1.2 Objectives

The main aim of this thesis is to develop an advanced polymeric composite which can effectively shield against fast neutron particles in a space environment. The objectives include:

- Finding potential neutron-shielding polymers and neutron absorbers through theoretical and experimental studies.
- Producing the desired polymer composite from the theory using the solvent casting technique and studying the experimental result.
- Analysing the shielding potential of the material against fast neutron energy through the pulse-height spectrometry.

To have a good understanding of the effects of neutron radiation on space mission, one needs to obtain general information on the primary radiation as well as the deeper information on the secondary neutron radiation. Compared to directly ionizing radiations, cosmic-ray neutron interacts with matter differently. Understanding the neutron behaviour will help a lot in the search of shielding material. Moreover, establishing the energy range of neutrons in space is essential, since different types of shielding material deal with different neutron energy ranges.

The theoretical selection of potential materials as well as their manufacturing method was illustrated. For neutron radiation, the development of polymeric composites to be used as a neutron shield has been suggested for several years. Reasons for this recommendation will be discussed in the theory section.. The selected material was created with suitable methods at Arcada University of Applied Science. The quantification of the composite's supernatant after the solvent casting experiment was studied using UV-Vis spectrophotometer. The working principle for this analysis method was reviewed in the theory section. Furthermore, the analysis on the neutron shielding potential of the composites will be investigated using pulse-height spectrometry from the neutron detector in the University of Helsinki. Since understanding the mechanism of the detector is key to understand the analysis, a brief theory review on it is included. Additionally, a brief history the discovery of cosmic radiation is discussed.

2 LITERATURE REVIEW

2.1 The discovery of radiation from outer space.

After the early work on radioactive matter on Earth was conducted by Marie and Pierre Curie through their experiment with Polonium and Radium (Angelis 2013), it was believed that the natural radioactivity with high-energy is created by heavy, unstable and radioactive elements and gases (Cosmic Ray 2019) or is detected from the soil (Angelis 2013) – the uppermost layer of Earth's crust. However, the major source of radiation had been discover to come from outer space, rather than from Earth. The discovery and study of natural radiations begun in the early 20^{th} century. In 1909, Theodor Wulf used electroscopes to measure the level of radioactivity at the top of the Eiffel Tower in Paris, expecting to measure a decreased rate. The results disproved his hypothesis and his paper was

not acknowledged back then (Angelis 2013). Similar results were found by Albert Gockel (a professor at University of Fribourg) and Karl Bergwitz's balloon experiment in 1909 when they sent the balloon flights at the altitude of 4000 meters and did not observe the decrease of ionization rate, as Gockel had expected based on the theory of a terrestrial origin (Angelis 2013). Unexpectedly, their work would lead to the discovery of cosmic radiation from space.

Domenico Pacini conducted an experiment in 1911 where he compared the rate of ionizing radiation at different altitudes above a lake, and under the water's surface. The result showed that there was a clear decrease in the amount of ionizing rate in the depth of water due to the absorption of its atomic component (Angelis 2013). Further confirmation was provided by Victor Hess's balloon experiments in 1912. In the final flight of the balloon experiment on the 7th of August, there was a significant increase in the ionizing rate through the measurement of radioactive absorption's coefficient as well as its variation's rate. Hess concluded that the radioactive source has an extra terrestrial origin, coming from above and increasing the rate proportional with the higher altitudes. The theory then later again confirmed by German physicist – Werner Kolhörster with the altitudes up to 9200 meters. This concluded that a significant increase of ionizing rate from an extraterresteriaorigin could be observed from 10 times above sea level (Angelis 2013). This confirms that other radioactive sources came from outer space as well.

2.2 Radiation

Radiation from outer space is one of the first, unavoidable threats for the mission of space exploration. Radiation is a type of energy that is diffused or transmitted in the form of rays, electromagnetic waves or particles. Radiation can be classified as ionizing or non-ionizing, which can act like waves or a stream of particles called photon with no mass (see Fig. 1). The shorter their wavelength, the higher their corresponding energy. Another type of ionizing radiation is primary galactic cosmic radiation (GCR) which possesses heavy-ion and high energy protons. GCR comes from outside the solar system, but is usually detected from Milky Way galaxy. Both types have enough energy to ionize an atom/molecule of a matter by eliminating an electron from its orbit. Being energetic enough to break apart atomic bonds, ionizing radiation poses a significant danger to space travel, in contrast to the non-ionizing rays encountered through daily activity such as

microwave or mobile phone. The direct effect of space radiation is to damage human cells and living tissues and to break down the DNA strands after the exposure (Johnson 2002). Cosmic radiation is associated with cosmic rays and solar flare particles, which come from the galactic space environment and the Sun's activity (Lloyd et al. 2017).

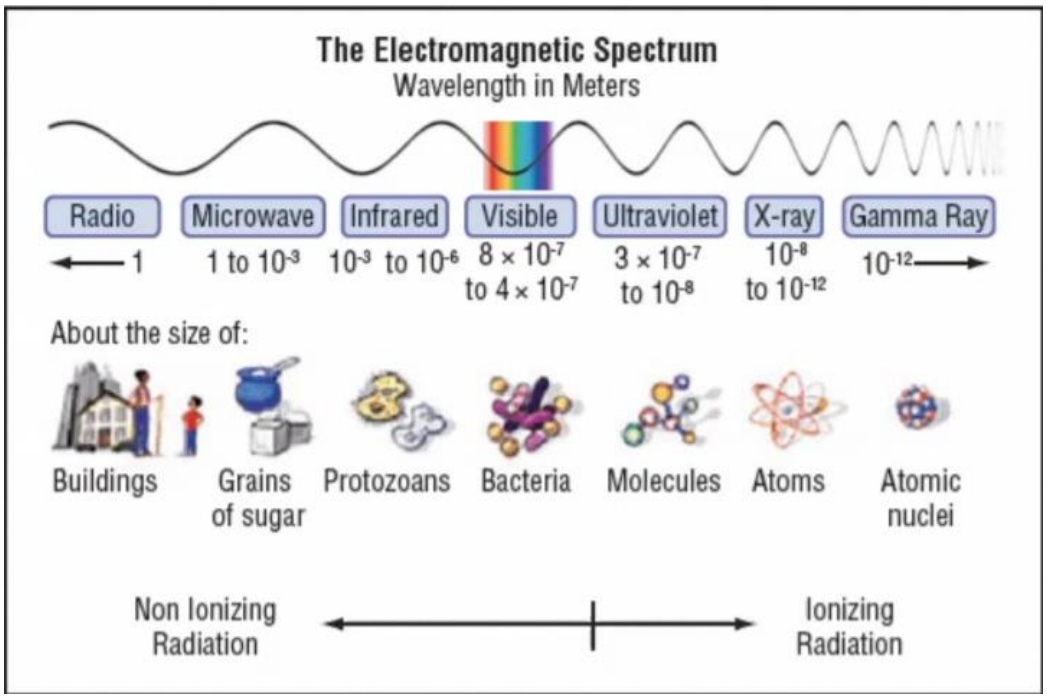

Figure 1. The Electromagnetic spectrum of non-ionizing and ionizing radiation (Lloyd et al. 2017).

According to Eckhardt (1995) and the US Federal Communications Commission (Cleveland & Ulcek 1999), the energy content of photon required to induce ionization and biological damage is over 10 eV. High-energy ultraviolet is the region where the ionizing energy takes place. It was discovered that the molecules of water or oxygen can be ionized at an energy of 12 eV while 15 eV is required for nitrogen molecules (Eckhardt 1995). Gamma radiation has the highest energy in the spectrum and starts from the energy of 100 keV. It has the potential to be greater than 1 MeV in the space environment. The energy range of ionizing radiation and radioactive matter is illustrated in Fig. 2, represented by Eckhardt:

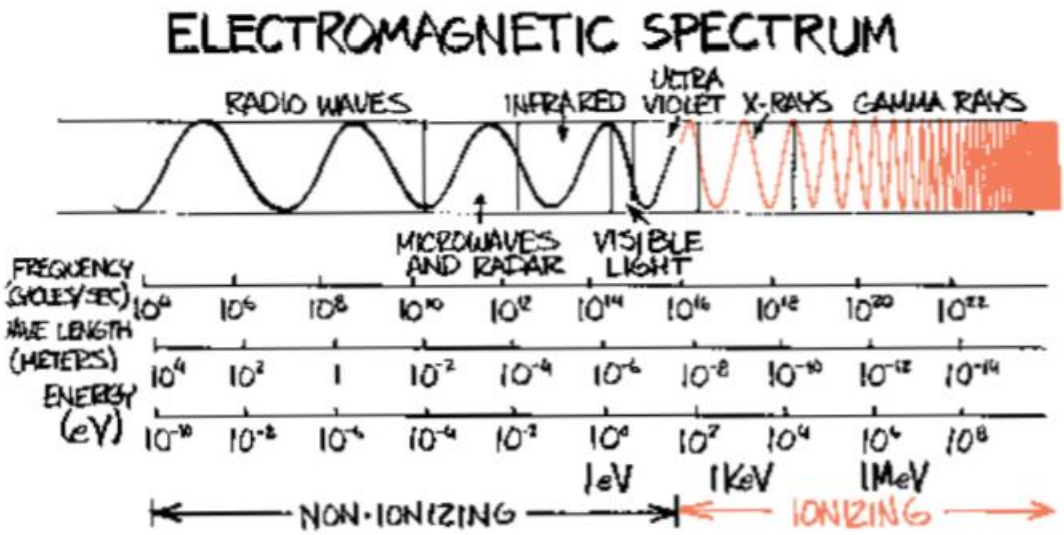

Figure 2. The energy range of the electromagnetic spectrum (Eckhardt 1995).

Ionizing subatomic particles can originate from galactic events such as supernova occasion (exploding stars), from the Sun's activities and the Van Allen Belt (Earth's radiation belt) (Lloyd et al. 2017). It was stated by Friedberg and Copeland (2011) that the solar wind can carry energies between 10 to 100 keV while Van Allen Belt can produce energy ranges from 10 – 100 MeV. It was also reported by NASA (What is space radiation? 2019) that the outer radiation belt consists of electrons with energies up to 10 MeV. Furthermore, while travelling in space, NASA estimated that astronauts suffer from an exposure dose of ionizing radiation in the range from 50 – 2000 mSv (Perez 2019). According to statistical and radiation studies, Satterfield (2009) reported that 5000 mSv is the estimate equivalent dose of radiation which could cause cancer and death to human.

2.3 Secondary neutron radiation

Neutron radiation was discovered by an English physicist James Chadwick in 1932 (Singh 2017). This was an enormous milestone in the studied history of atomic physics since it provided a deeper understanding of the structure of an atom and its working mechanism. In 1931, two German scientists announced that abnormally powerful radiation – thought to be gamma – was created by the interaction between certain elements (beryllium or boron) and the alpha particles radiation's decay from Polonium. Having doubts about their experimental result, Chadwick replicated the test and analysed again the final observation. In his case, paraffin wax was used to capture the emitted radiation after the

reaction. In further analysis, this unidentified radiation was observed to scatter the protons at a different angle as compared with gamma rays and to have a net neutral charge. Chadwick also observed that it had a similar mass to protons. The unusual radiation was named neutron. In 1935, Chadwick received the noble prize for his discovery (Singh 2017).

Primary ionizing radiation can cause cancer and death since they have strong energy which can penetrate deeply into matter's structure, damaging and preventing human cells from regenerating (Rogers 2009). They are called direct radiation and are made of charged particles (Cherry n.d.). Another type of ionizing rays – econdary radiation – is a major focus of this thesis. These can be positive, negative or neutrally charged particles and can also be understood as indirect ionizing radiation since they are created from the interaction of direct radiation with matter through Coulomb force (Cherry n.d.). Specifically, the shielding against neutron radiation will be studied in this thesis. Cosmic neutron radiation has been reported to be more threatening due to their electrically neutral characteristic, leading to a higher level of exposure and penetration. Johnason (2002) also reported that the blood-forming marrow in bones can be strongly damaged by neutron radiation.

2.3.1 Neutron interaction mechanism

Neutron radiation exists as free neutron, which is created when radiation strikes an atomic nucleus, splitting and ejecting its proton and neutron components (secondary effect) (Johnson 2002). By this way, neutron particles present not only in space vehicles but also on the Moon and Mars' surface (Thibeault et al. 2012). When neutron is created, it is given enough energy to affect the neighbour atoms of matter, breaking apart the nucleus and release extra free neutrons from atoms, protons and pions (Friedberg & Copeland 2011). Free neutrons are unstable and will decay in around 10.6 minutes by the beta minus decay if no interaction occurs (What are Cosmic Rays? 2019).

Although neutron radiation has a short life, it is more dangerous when encountering matters as compared to alpha, beta or even gamma rays (Neutron Radioprotection n.d.). Fig.3 shows that neutron radiation only loses its energy due to the collision with matter's nucleus (What are Cosmic Rays? 2019). Since it does not interact with matter's electron as other types of radiation do, it can penetrate deeper and cause greater damage to matter whose structure has a low neutron cross-section (e.g. heavy metals). During long-term

space missions, multiple types of radiation will be encountered. In this environment, there is a significant probablilty of generating neutron particles.

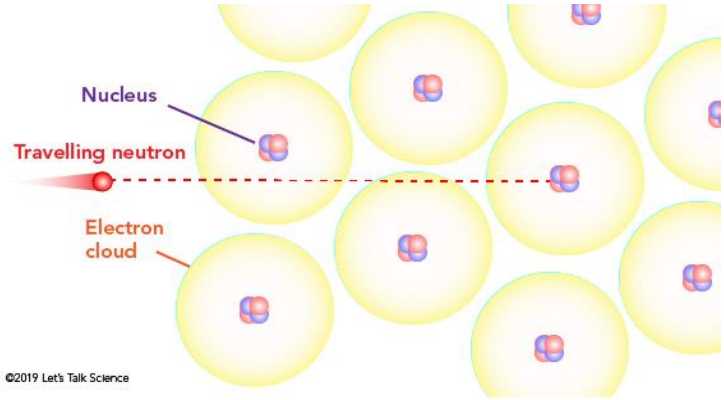

Figure 3. Neutron radiation interacts with the nucleus of matter (What are Cosmic Rays? 2019).

Similar to other primary rays, neutron radiation undergoes two types of interaction when it encounters physical shielding material: scattering and absorption. When meeting high-energy (fast) neutron, scattering interaction is more likely to happen than absorption (McAlister 2016). Scattering phenomenon can be divided into two groups: inelastic and elastic scattering. Inelastic happens when the target nucleus is increased to a quantum state, giving it the energy to be excited above the ground level. The kinetic energy of the neutron-nucleus system is lower through this phenomenon, making the nucleus decay to the ground state by the emission of gamma rays. On the other side, the kinetic energy of elastic scattering is conserved, where the energy level of the target nucleus remains the same as before the collision (Selph et al. 1968, p. 259-260).

The interaction process of neutron and nucleus can lead to an increase in damage on the atom and alter its character. Neutron particles can strike protons out of its original position in the atom, creating enough energy for protons to travel a short distance and affecting nearby atoms with an amount of ionization. An atom can lose protons and absorb neutron particles, becoming an unstable and heavier radioisotope. Because of this influence, nuclear excitation phenomena will occur, where other additional types of ionizing radiation such as gamma rays can be induced by a neutron particle (Friedberg & Copeland 2011). Taking the reaction of neutron energy and element boron as an example. One of the stable isotopes of Boron – $^{10}_{5}\mathrm{B}$ (19.9% isotopic abundance) – is widely used as neutron absorber because of its high neutron cross-section. According to Révay et al. (2011), the boron-

thermal neutron reaction carries out by not only an alpha particle and lithium recoil nucleus, but also 94% of neutron absorbed energy by element $^{10}_{5}\mathrm{B}$ can generate the gamma radiation energy of 0.478 MeV from $^{7}_{3}\mathrm{Li}^{3+}$. The reaction equation was demonstrated by Fisher et al. (2011):

$$^{10}_{5}\mathrm{B} + {}^{1}_{0}\mathrm{n}_{\mathrm{th}} \rightarrow {}^{4}_{2}\alpha(1.47\ \mathrm{MeV}) + {}^{7}_{3}\mathrm{Li}(0.84\ \mathrm{MeV}) + \gamma(0.478\ \mathrm{MeV})(94\%) \qquad (2.3.1.1)$$

2.3.2 The energy range of neutron radiation in the space environment

A board range of neutron energies created by the interaction of GCR ions in space environment can vary from eV to GeV (Köhler et al. 2015). According to Connor (2019), neutron energy can be classified into various groups based on their kinetic energy. For simplification, there are three main groups of neutron energy spectrum: slow/thermal neutrons having the lowest range of energy (0.025 eV – 1 eV), resonance neutrons (1 eV – 1 keV) and fast/fission neutrons having the highest range of energy (1 keV – 10 MeV). Connor then illustrated the energy range through Fig. 4:

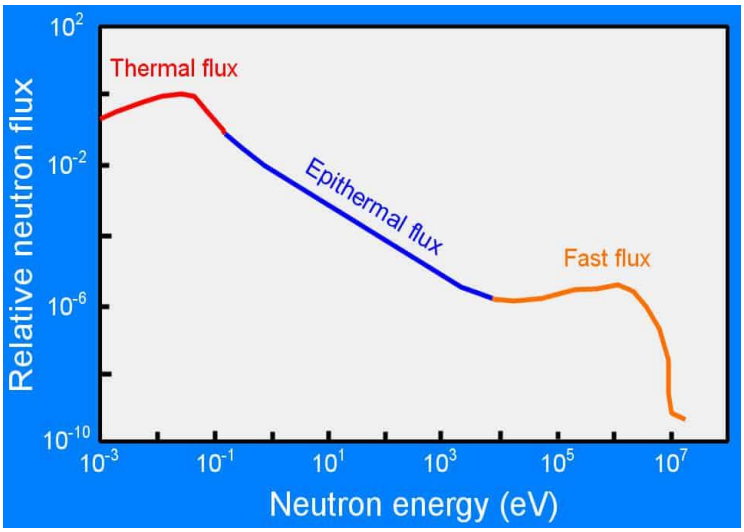

Figure 4. The illustration of the Neutron energy spectrum (Connor 2019).

Based on Connor's classification of neutron energy, cosmic neutrons found in space environment were observed to be in the range of 100 keV – 1 MeV, fast (1 MeV – 20 MeV) and relativistic (< 20 MeV) neutrons. The spectrum of the cosmic-ray neutron was studied in detail by Nakamura (2008) at several different altitudes: sea level, 4.88 km and 11.28 km above the Earth's surface. The energy range of neutron radiation onboard the ISS at the altitude variation of 300 – 500 km was also examined by Koshiishi et al. (2007).

Finally, Köhler et al. (2015) further performed a similar measurement of neutron energy in transit to Mars.

The neutron radiation spectrum in space environment at different altitudes (above the sea level) was measured by Nakamura and through the report of Goldhagen et al. (2008). The analysis of neutron energy aboard an airplane and in space had been experimented by using a balloon, space shuttle and space station. The applied detector called Bonner Ball is a multi-moderator spectrometer. At the solar minimum period in 1985, the measurement of neutron energy had been performed by flying at an altitude of 4.88 km for 60 minutes (Nakamura) and 20 minutes at 11.28 km (Goldhagen, et.al.). To collect the data at an altitude of 4.88 km, the Bonner Ball with five polyethene moderators, built by Nakamura and Uwamino, had been used while the Bonner Ball developed by Goldhagen, et.al. with 14 detectors had been applied for the measurement at 11.28 km. In 2002, at solar maximum period, a balloon had been used to obtain the neutron energy data at sea level (70 m). The neutron spectrum and dosimetry at the altitude of sea level, 4.88 km and 11.18 km had been represented through Fig. 5 by Goldhagen, et.al. and Nakamura as below:

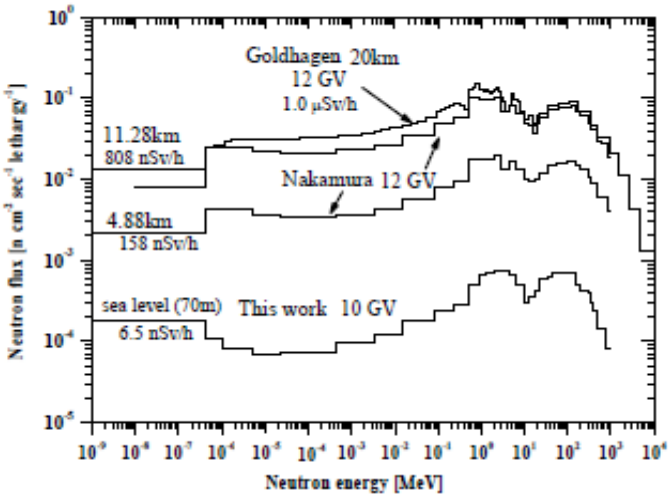

Figure 5. The neutron energy illustration of Goldhagen, et.al. and Nakamura (2008).

Fig. 5 showed the similarity of the cosmic-ray neutron spectrum in comparison of three tests. It can be observed that there are three major peaks within three performed tests: thermal peak (1 eV), evaporation peak (1 MeV) and cascade peak (100 MeV). At three altitudes, the neutron energy was detected to be in the range from 1 MeV to 100 MeV. To measure accurate data of the neutron flux and ambient dose, it is significantly depending on the altitude and latitude. Moreover, in 1998, the similar type of Bonner Ball

manufactured by National Space Development Agency (NASDA) had been installed in the SPACEHAB module in the space shuttle cargo bay (STS-89) to measure the neutron energy spectrum within the South Atlantic Anomaly (SAA), polar and equatorial regions. Fig. 6 demonstrated the data for the case. The total neutron fluxes of three regions equivalent to an amount of neutron energy were reported. Nakamura observed that the neutron fluxes of Equatorial and Polar regions fluctuated from $0.35 - 7.97\ \mathrm{cm^{-2}s^{-1}}$ while SAA region results in an amount of $7.64 - 112.95\ \mathrm{cm^{-2}s^{-1}}$. The measurements were then calculated to obtain the average dose equivalent rates, which were $3.01\ \frac{\mu Sv}{h}$ for Equatorial and Polar region and $45.8\ \frac{\mu Sv}{h}$ for SAA regions. (Nakamura 2008)

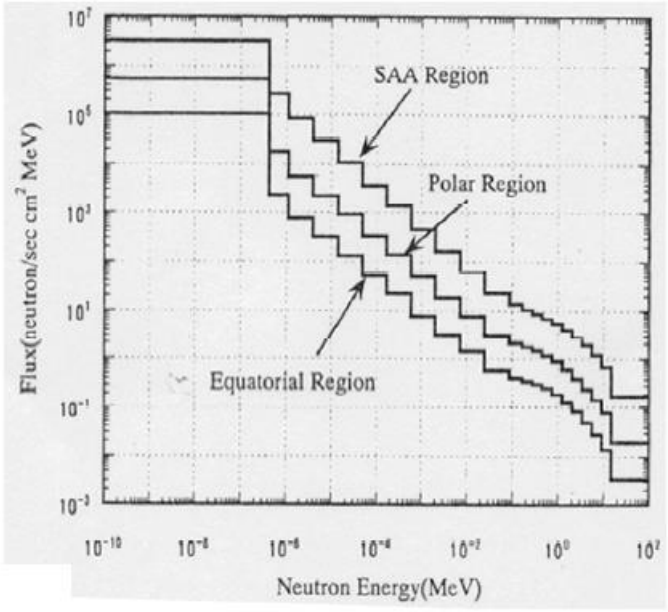

Figure 6. The spectrum of neutron energy was measured by the use of Bonner Ball in space shuttle STS-89 (Nakamura 2008).

The energy spectrum and dose equivalent of neutron radiation existed in the ISS have been also measured by Koshiishi et al. (2007). As it was mentioned in Nakamura's article, Bonner Ball neutron detector with six sensors used on the space shuttle STS-89 in 1998 had also been mounted inside the US module of the ISS by NASA in 2001. The detector had been further applied to investigate the neutron energy spectrum presented on the ISS (reported altitude 300 – 500 km). Onboard of the ISS, it had been discovered that most of the neutrons were secondary particles created by the interaction process of primary radiations and matters, rather than cosmic sources such as supernovae. The experiment had been performed by relocating the Bonner Ball in various locations on the ISS to measure

the most accurate data of neutron spectrum. Depending on each location with different shielding layers and compositions, the neutron radiation atmosphere inside the ISS was detected to vary its thermal energy up to 15 MeV in the maximum period of solar activity. In this period, it had been measured that the energy alternation of the orbit-averaged neutron range was larger than 10 keV. From the data, astronauts might be exposed to a neutron dose equivalent of 69 $\frac{\mu Sv}{day}$ and 88 $\frac{\mu Sv}{day}$ at two locations, resulting in a difference of 30%. The record could be affected by the altitude variation of the ISS (increase by the factor of 2) and the shielding condition. Furthermore, the changing of the shielding thickness as well as the solar activity could also impact the data. The efficient thickness of a shield on the ISS was recorded to be $20 \frac{g}{cm^3}$. (Koshiishi 2007)

Additionally, the analysis of the neutron spectrum in transit to Mars had been evaluated by a team of researchers from the Mars Science Laboratory (MSL) (Köhler et al. 2015). This serves the purpose of the interplanetary study as well as the investigation of radiation aspect for the mission to Mars. The measurement had been accomplished by using Radiation Assessment Detector (RAD) mounted inside the MSL spacecraft and launched to Mars in 2011, onboard with the Curiosity rover. The detector had been applied to not only quantify the neutron exposure on Mars's surface but also in the transition to Mars, accounted for 253 days with 56×10^7 km. Scientists had applied RAD's measurement of neutron particles to calculate the neutron spectra impacting on the spacecraft's shielding performance. From the estimation and mathematic calculation, the neutron spectrum could be plotted by Köhler et al. (2015) in Fig. 7.

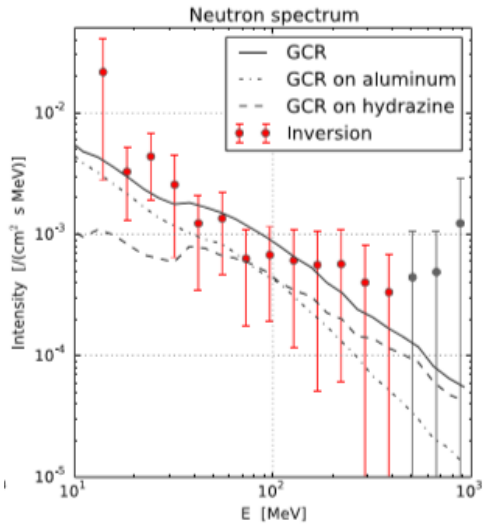

Figure 7. The measurement of neutron spectra with the interaction results of individual GCR, GCR on aluminium and GCR on hydrazine (Köhler et al. 2015).

The data illustrates the behaviour of neutron energy on the hydrazine tanks and aluminium – the two main compositions of the spacecraft's shield. Köhler et.al. (2015) had claimed that the neutron spectrum induced by the interactions of GCR on two materials could be estimated through simulation. To perform the measurement, GEANT4 Monte Carlo code was used. The energy variation of 10 – 1000 MeV for neutron spectra's incident was chosen for modelling the data. Using the inversion technique, Fig. 7 shows the spectra of neutron radiation which presented during the transit to Mars (approximated energy range of 12 – 436 MeV). This led to a neutron dose equivalent and dose rate of $19 \pm 5\ \frac{\mu Sv}{day}$ and $3.8 \pm 1.2\ \frac{\mu Gy}{day}$ respectively. For further investigation, the simulation of energy variation had been extended (0.1 – 1000 MeV) to observe the changing dose equivalent and dose rate, producing results of $30 \pm 10\ \frac{\mu Sv}{day}$ and $6 \pm 2\ \frac{\mu Gy}{day}$.

2.4 The proposal of polymer composite as neutron-shielding material

In addition to the heavy metals, aluminium alloy that is traditionally applied to attenuate the space radiations is also one of the most well-known long-established materials. It has played an important role in the history of the aerospace industry in numerous space missions. For instance, aluminium alloy had been applied to manufacture the first artificial Earth satellites – called Sputnik 1 – by the Soviet Union in 1957 (Imster & Byrd 2019). Aluminium has been used widely for the application of spacecraft, satellites, or space probes for the study of Earth or Solar System's planets, planetary satellite and asteroids. Up to now, aluminium and its composites are the typical materials for space technologies, such as the window shutters of ISS because of its strength while remaining light-weight structure at the same time (What Materials Can Survive in Space? 2019).

However, producing a neutron-radiation shield from traditional materials seems to be an impractical solution for long duration space missions. Having the protective layer made of heavy metals not only provides a cumbersome structure but also increases the probability of generating secondary radiations (Nambiar & Yeow 2012). Since heavy elements with high atomic number have a low neutron cross-section, they are impractical for human long-term interplanetary spaceflight in the shielding against cosmic-ray neutrons. Various extra shielding layers might be required, leading to an increase in cost and weight of the structure (Nambiar & Yeow 2012). Elements such as hydrogen, carbon, oxygen

and nitrogen, having lower atomic numbers with high neutron scattering cross-section are the most efficient candidates in moderating and thermalizing incident thermal neutrons (McAlister 2016). Neutron energy can be reduced by the elastic collision with a light atom, especially hydrogen (Kiefer 2011). Hydrogen is the most advantageous element which is well-known for effectively scattering and slowing down neutron particles (Jumpee & Wongsawaeng 2015). As a hydrogen rich compound, water can make an excellent and easily applied shielding material. However, the usefulness of water shielding for space applications is reduced due to the presence of heavier oxygen atoms which increase weight and launch cost (Marshal 2007).

Polymer composites fulfil most of the mission's requirements by being extremely lightweight, high-strength, effective, economical and flexible. It is an attractive material in neutron radiation shielding (Nambiar & Yeow 2012). This advanced material has been tremendously studied and developed by scientists in the search for an efficient neutron shielding material. Containing three efficient elements: hydrogen, carbon and oxygen, it has been proved that one of the hydrogen-rich polymers – Polyethylene (PE) – was 15% and 50% better at shielding GCR and solar flares than aluminium (Marshal 2007). Due to reduced mechanical strength, when compared to traditional metals, polymers can not always perform effectively in the harsh space environment for long periods. Furthermore, polymers can only restrict and well-tolerated neutron energy, rather than stopping completely the neutrons. To improve this weakness, the idea of introducing an inorganic compound (neutron absorber) into pure hydrogen-rich polymer matrix has been proposed and experimented for several years. Having a high neutron captured cross-section, the neutron absorber can capture completely neutrons as well as reinforced polymer's mechanical strength while still being well-distributed in their matrix. Theoretically, this creates a new type of polymer composite for neutron radiation shielding, protecting the space structure as well as astronauts from neutron exposure.

2.4.1 Neutron Absorber

As discussed, introducing neutron absorbers into the polymer matrix can improve polymer weakness. The most well-studied elements for this purpose are lithium, boron, cadmium and gadolinium because they are four of the elements which have a very high neutron capture cross-section in nuclide chart. In practical cases, these elements which are

usually applied for nuclear reactor purpose has been reported to show a great efficiency in stopping neutron radiation. However, a flawless and ideal shielding material does not yet exist. Although they show potential, side effects are observed with these materials after interaction with radia-tion. A shield that absorbs all the neutron's energy can also produce secondary radiation or residual radioactivity. Similar to the case of boron as described in section 2.3.1, cadmium and gadolinium can also produce gamma radiation after their thermal neutron reaction. However, it is acknowledged that the greater energy of gamma-ray will be created by cadmium's and gadolinium's reactions as compare to boron's since both are heavy metals. The reaction of the thermal neutron particle with Cadmium had been illustrated by Murray and Holbert (2019) while Tanaka et al. (2019) had illustrated the nuclear equations of gadolinium.

Cadmium

$$^{113}_{48}\mathrm{Cd} + {}^{1}_{0}\mathrm{n} \rightarrow {}^{114}_{48}\mathrm{Cd} + \gamma \text{ rays} \qquad (2.4.1.1)$$

Gadolinium $^{155}_{64}\mathrm{Gd}$

$$^{155}_{64}\mathrm{Gd} + {}^{1}_{0}\mathrm{n} \rightarrow {}^{156}_{64}\mathrm{Gd} + \gamma \text{ rays } (8.536 \text{ MeV total}) \qquad (2.4.1.2)$$

Cadmium, gadolinium, or other heavy metals which have excellent neutron cross-section capture are widely used for nuclear applications. On Earth, various layers can be added to shield against gamma rays in nuclear reactor and weight is not necessarily an important factor. However, as discussed above, using heavy metals as a neutron shield is impractical for long-term mission in space. For neutron radiation-shielding in space, neutron with low energy can also be absorbed effectively by boron (isotope $^{11}_{5}\mathrm{B}$ or $^{10}_{5}\mathrm{B}$) and lithium (isotope $^{6}_{3}\mathrm{Li}$) without producing high energy gamma rays as compare to other heavy elements. Lithium and boron show the best potential for the space technology, although neither possess neutron capture cross-section as large as cadmium and gadolinium. The cross section of cadmium and gadolinium isotopes account at 20.600 barns and 60.900 barns while boron has 3838 barns and only 941 barns for lithium (Révay et al. 2011). Despite the theoretical limitations, boron and lithium are still considered to be more advantageous in the shielding against cosmic-ray neutron. In the development of neutron shielding

material, the concept of using B_4C and BN compounds as neutron capturers are widely applied.

Beside boron, lithium compounds (lithium fluoride, lithium carbonate, etc...) can also be the potential neutron absorbers. An advantage of using lithium compounds is that lithium can effectively absorb neutron particles without generating high-energy gamma rays. When interacting with a thermal neutron, lithium fissions into alpha and tritium particles, releasing roughly the total energy of 4.78 MeV. The lithium-thermal neutron chemical reaction was demonstrated by Fisher et al. (2011) as below:

$$^{6}_{3}\mathrm{Li} + {}^{1}_{0}\mathrm{n} \rightarrow {}^{3}_{1}\mathrm{He}\ (2.05\ \mathrm{MeV}) + {}^{4}_{2}\alpha\ (2.73\ \mathrm{MeV}) \qquad (2.4.1.4)$$

To our best knowledge, lithium isotope has not been widely used for this concept. No article was found on the introduction of lithium compounds into the polymeric matrix for the shielding against neutron radiation. Since the neutron cross-section capture of lithium is such significantly smaller as compare to boron, this creates inefficiency for the application. Moreover, the nuclear reaction between lithium and thermal neutron causes unstable tritium. These two disadvantages of lithium element reduce its attractiveness as a neutron absorber in the polymer matrix.

2.4.2 Polymer

For shielding against the cosmic neutron, aliphatic polymers have always been the desirable selection because of their high hydrogen content. In recent papers, the concept of using PE had a great influence on numerous studies for this specific shielding application. According to Soltani et al. (2016), a brief study of high-density polyethylene (HDPE) with boron carbide nanocomposite (HDPE/B_4C) as the neutron shielding material had been reported to possess an efficient shielding potential, low weight with a thin layer and cost-effective performance. Furthermore, the research performed by Shin et al. (2014) had also shown great shielding efficiency. A neutron shield made of the HDPE matrix with modified boron nitride (HDPE/mBN) has a greater shielding performance, tensile modulus and thermal conductivity as compared to low-hydrogen content polymers. Eventually, aliphatic polymers were the first choice for thesis research.

On the other side, aliphatic hydrogen-rich polymers have some drawbacks. According to Özdemir et al. (2017), HDPE had been demonstrated to be inflexible. The lack of flexibility of the shielding material creates some disadvantage (fast shaping as an example) on its performance during the normal operation of the space mission (Özdemir et al. 2017). Moreover, due to the high hydrogen content, aliphatic polymers do not possess the essential thermal and mechanical strength for space exploration, resulting in poor durability. As stated by Castley et al. (2019), the current concept of using hydrogen-rich polymers such as PE, polypropylene (PP) or polyamide (PA) incorporate with neutron absorbers (lithium or boron) might have restricted the temperature resistant up to $200℃$. To address the problem, Özdemir et al. (2017) had suggested the application of ethylene propylene diene monomer (EPDM) rubber composite in exchange of PE, resulting in better material flexibility since the hydrogen content of EPDM rubber is 8.6% less than HDPE. It had been desmontrated that EPDM rubber with boric trioxide (B_2O_3) composite gained better flexibility, tensile strength and tear resistance (Özdemir et al. 2017). However, the existence of ethylene and propylene in the main chain of EPDM rubber might encounter the problem that had been addressed by Castley et al. (2019).

To avoid the drawback of aliphatic polymers, aromatic polymers are a good alternative that can be used in space application. According to Bate (2009), the aromatic backbones of a polymer provide greater mechanical strength, well-tolerated radiation, and higher thermal stability than aliphatic polymers. These advantageous abilities make aromatic polymer attractive to this thesis. In his study, polyimide (PI) had been used and demonstrated to have good thermal property, chemical resistance, mechanical strength and some extensive applications for space technology (Bate 2009). However, the disadvantage of this type of polymer is due to the low hydrogen content, especially for the shielding production against neutron radiation. Bate (2009) had then suggested either forming the hydrogen-rich monomers from which to synthesize the polymers or introducing more weight percentage of neutron-capture element into the polymer's matrix. In this way, the drawback of aromatic polymers can be reduced.

2.5 The use of solvent casting technique on the production of polymer composite

In the study of neutron-shielding materials used in the space environment, there are many ways to manufacture the desired polymer composite from organic polymer and inorganic neutron absorber. The constituents of the composite can be melted and blended. This type of mixing method had been used in various articles. For example, Herrman et al. (2019) manufactured PE/B_4C and PE/BN through the blending process using injection moulding machine. Zahra et al. (2016) used a commercial extruder to mix the blended HDPE granules with B_4C powder together, creating a uniformly distributed HDPE/B_4C composite. Many other studies have also applied the mixing method to obtain a homogeneous composite. However, this method requires cumbersome machines to perform, such as an extruder, injection moulder or two-roll mill.

The solvent casting method has been proposed by Li et al. (2018) to investigate a new neutron-shielding polymer composite for nuclear application. This method was a good and simple alternative to create the desired polymer composite for this thesis. Li et al. (2018) studied the potential of the incorporation of B_4C within the PI matrix as a shielding composite for the neutron protection in the nuclear application. To achieve a homogenous structure of PI/B_4C composite, PI was synthesized from scratch using Biphenyl dianhydride (BPDA) and 4, 4′-Oxydianiline (ODA). The polymerization was accomplished by the temperature control of the thermal-imidization process. At the same time, the surface modification of B_4C and solvent casting method had been applied. At the end of the production process, B_4C had been dispersed homogeneously in the PI matrix, creating a well-characterized PI/B_4C composite with superior thermal stability and mechanical durability. The procedure is summarized in Fig. 8.

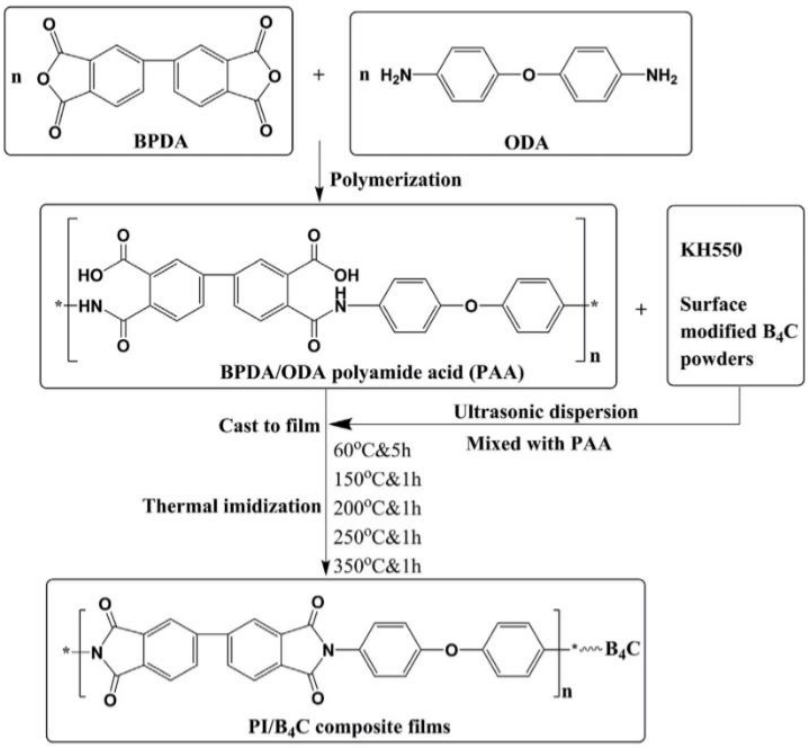

Figure 8. The synthesized method of Polyimide/Boron Carbide composite (Li et al. 2018).

The solvent casting method is one of the oldest and most efficient technologies used in the plastic film production industry. The method was established more than hundred years ago (Siemann 2005, p. 1) and has become extremely useful in the manufacturing of polymer film, fulfilling the demand for material's high quality nowadays. Having the advantages of uniform thickness distribution, maximum optical purity and extremely low haze (Siemann 2005, p. 1), solvent casting is an attractive technique used mainly for manufacturing polymer composite films. The process involves using a solvent to dissolve the constituents and create a new homogenous structure from these raw materials. In the end, the solution is left to evaporate the remaining solvent, leaving a new uniform structure of polymer composite film made from organic and inorganic compounds. Furthermore, the process of solvent evaporation can be accelerated using the method of heating, or simply placing the solution in a vacuum environment. Fig. 9 illustrates of the solvent casting technique:

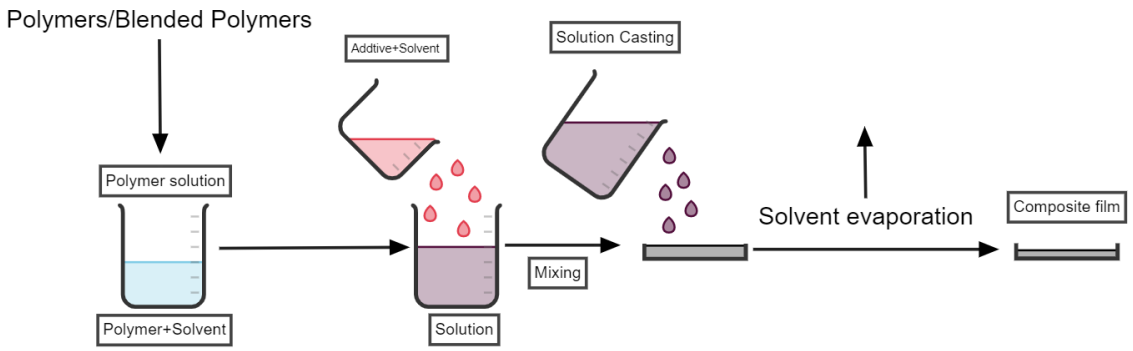

Figure 9. Schematic illustration of solvent casting technology (2020).

According to Christesen (2011), the disadvantage of this method is that the solvent can remain within the composite matrix even after drying/evaporation process. It acts as a plasticizer which enhances the plasticity or fluidity of the composite. This will make the material softer, resulting in the dramatic decrease in material strength. A small amount of solvent remaining in the final material can drastically reduce performance, leading to a loss of mechanical strength and overall practicality. The impact of the solvent can cause the composite to become softer or swollen.

2.6 Ultraviolet-Visible Spectrophotometer for the quantitative analysis of the experimental supernatant

A UV-Vis spectrophotometer was used for experimental purposes later in this thesis. The spectrophotometer is the most appropriate technology in the study of chemicals' concentration of a solution or a gas phase. It is a quantitative analytical instrument that measures the absorption rate of chemical compounds based on the electromagnetic spectrum of near-ultraviolet (wavelength from 180 nm to 390 nm) and visible-light (wavelength from 390 nm to 780 nm) radiation. An amount of energy coming from the light source interacts with sample's molecules/atoms, increasing electron transition of the chemical compounds. The spectra are created when the electrons of molecules travel from lower to higher energy. Based on their theoretical absorbance properties, the near-UV spectrum is usually the most appropriate for identifying organic compounds, whilst the visible spectrum is used for inorganic compounds (Worsfold & Zagatto 2019).

To obtain a better understanding of the UV-Vis instrument's operation, Fig. 10 demonstrates its fundamental working principle. A beam of light comes from the ultraviolet spectrum source (or visible source), travels to a slit and hits the diffraction grating, where

polychromatic light will be separated into monochromatic light at different and selected wavelengths. Each monochromatic beam (single light) travels to a modulator, where it is separated into two equal intensity beams. A filter may be applied to eliminate unwanted diffraction. One beam then passes through the studied sample cuvette and the other passes through an identical cuvette contining only the solvent (Fallon 2012). The intensity travelled through two cuvettes is measured, analysed and compared by electronic detectors and its software. The spectrophotometer will then scan all wavelengths.

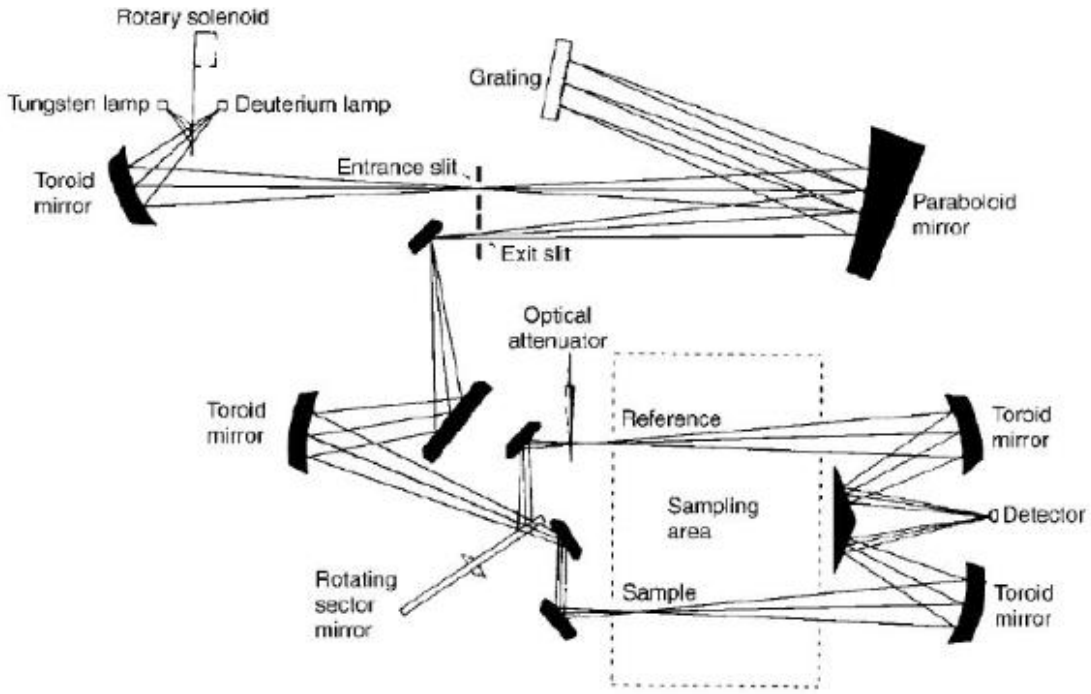

Figure 10. The light path of UV-Visible spectroscopy (Fallon 2012).

The principle of the instrument based on Beer's law, which describes the relationship of the sample's light absorption versus its concentration and path length. When a beam of radiation travels through a solution, different wavelengths of light are absorbed or transmitted through the sample. The initial intensity of light before encountering the sample has the symbol of I_0, whether the final intensity of light will be varied after passing through the sample, called I. The ratio of $\frac{I_0}{I}$ at a specific wavelength is determined as the transmittance (T). Principally, the negative logarithm of the transmittance describes the absorbance (A) of the solution. The theory could be simplified through Eq. (2.6.1) (Fallon 2012)

$$A = \log_{10}(\frac{I_0}{I}) = \varepsilon \times l \times C \quad (2.6.1)$$

Where

- A is the absorbance (no unit)
- ε is the absorption coefficient of the solution ($\frac{l}{mol \times cm}$)
- l is the length of the path light travelling in the solution (cm)
- C is the concentration of the solution ($\frac{mol}{l}$)

Fallon (2012) had represented the law idea through Fig. 11. A single wavelength of light passed through the solution can identify its concentration, along with the sample's path-length and absorptivity at a particular wavelength.

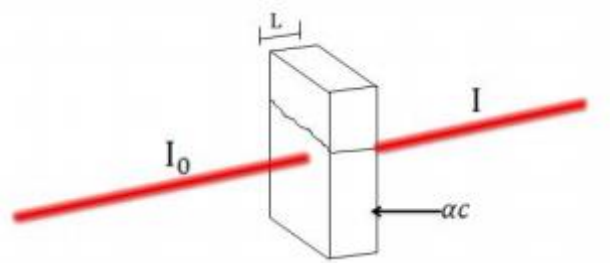

Figure 11: The illustration of Beer's Law applied in UV-Visible spectrophotometer (Fallon 2012).

2.7 Neutron detector

Neutron detector is the most important device in detecting the amount of fast (or thermal) neutrons before and after the shielding process from the neutron source. Many types of detector are used for this purpose which based on the nuclear reaction of each element. One can use boron trifluoride detector which based on ${}^{10}_{5}\mathrm{B}(n, \alpha)$ reaction or helium detector based on ${}^{3}_{2}\mathrm{He}(n, p)$ reaction. In this thesis, the plan was to use the helium tube. In this section, the working principle of this detector is briefly described.

Neutron radiation is special since it can not directly ionize gas molecules the same way as primary radiations. It can only ionize the atom indirectly through the product from the nuclear reaction. When a neutron collides with a nucleus of gas, the electrically charged proton is produced, ionizing other gas atoms. Based on this mechanism, helium is one of the most chosen elements for the neutron activity's detection. It not only is a light, reactive and high-electronegative nucleus but also has high sensitivity and cross-section to the interaction with neutron radiation. In the study case, the detector uses helium (isotope

$^{3}_{2}$He) as a converter gas to interact with the incoming neutron particles. This induces the ionization process, whose reaction was described by Knoll (2010) as below:

$$^{3}_{2}He + ^{1}_{0}n \rightarrow ^{1}_{1}H + ^{3}_{1}H \ \frac{Q - value}{0.764\ MeV} \qquad (2.7.1)$$

The reaction is called the (n, p) reaction. Two daughter products generated from each thermal neutron-helium nucleus reaction are proton and tritium. The reaction deposits an amount of product's energy of 0.764 MeV, called the Q-value. Q-value is carried in the form of kinetic energy and moves to the opposite direction of the daughter products with energies of 0.573 MeV (proton) and 0.191 MeV (tritium). The thermal neutron cross-section for this reaction is 5330 barns. (Knoll 2010)

When the nuclear reaction occurs, some molecules of the helium gas are ionized which creates ion pairs: charged ions (proton and tritium) and free electrons. At the same time, a high voltage is connected to the anode side of the detector to create a strong electrical field. Due to the strong acceleration caused by the field, positive ions are moved to the cathode while free electrons are pushed to the anode. As approaching the anode, the strength of the electrical field increases. Exponentially, free electrons are provided with sufficient energy to collide with additional helium atoms, which gives out extra positive ions and electrons, thereby ionizing those atoms. The process will continuously release more free electrons which interact with further atoms and creates more ions and electrons. Eventually, the effect produces further secondary ion pairs – called avalanche as they move closer to the anode. The phenomenon is called "the gas multiplication effect" (Geiger–Müller tube 2019). Furthermore, the surrounding helium atoms are also ionized by positively charged ions (proton and tritium). This produces more charged particles, which continuously ionize other helium atoms. The process is described as an avalanche-like multiplication which occurs within the helium detector (El-Batanouny 2020, p. 190). The sudden production of multiple avalanches from the nuclear reaction will trigger the normal avalanche process of the detector, thus providing the electronic pulse data through the read-out.

Some undesirable phenomena can occur during the process and can be observed through the spectrum. Two common influencers are called the wall effect (happens to slow and fast neutron detection) and elastic scattering effect of the neutrons from helium nuclei (only happens to fast neutron detection). The wall effect happens when the reaction of the

daughter products (proton and tritium) impacts on a larger range as compared with the dimension of the helium tube. It describes how the continuum spectrums (see Fig. 12) can be caused by the collision of protons or tritia with the detector's wall. The results are that their energy will dissipate and not contribute to the full-energy peak. (Knoll 2010)

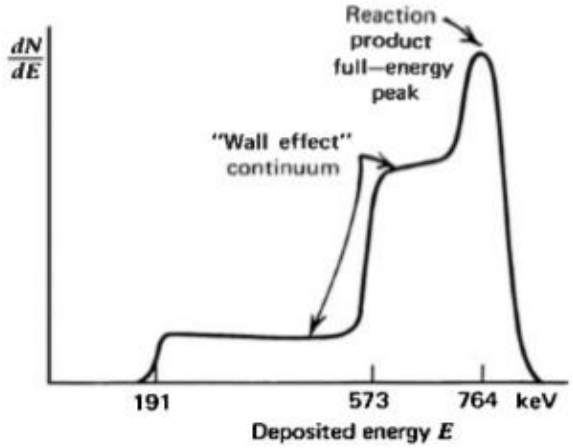

Figure 12. The expected pulse-height spectrum from a helium detector tube, where wall effect can be observed significantly (Knoll 2010).

For the fast neutron detection, the range of (n, p) reaction is usually recorded to be much smaller as compared with the cross-section of elastic scattering effect. This predominance can be very noticeable as the neutron energy rises rapidly. The essential features of the helium tube are accounted for by the reaction as well as the scattering effect. Fig. 13 illustrates the three discrete features of the helium tube in detecting the fast neutron. (Knoll 2020)

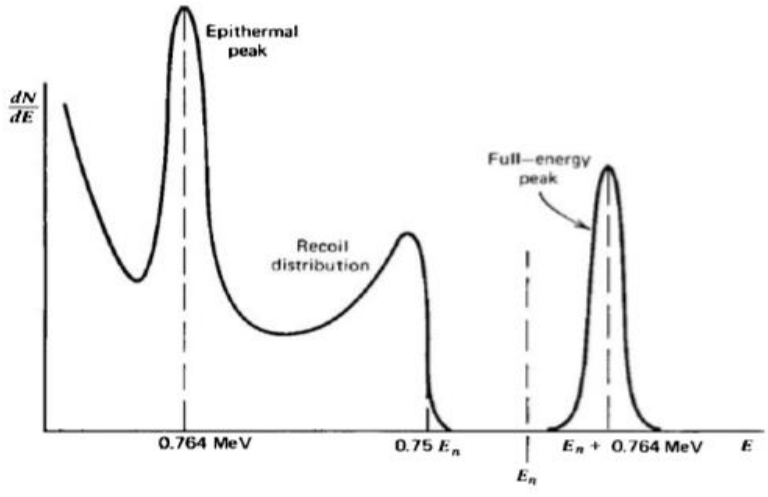

Figure 13. The expected energy spectrum from fast neutrons incident on the helium detector (Knoll 2020).

Due to the moderation in some external materials, some incident neutrons are reduced to the thermal range. The energy of these neutrons is represented as the epithermal peak at the Q-value energy. The second feature is the continuum spectrum (recoil distribution). The spectrum is observed due to the result of neutron elastic scattering effect and because neutron energy is partially transferred to a recoiling helium nucleus. The final feature is the full-energy peak. It is the representation of all the (n, p) reactions which are generated by the incident neutrons (Knoll 2010).

3 MATERIALS AND METHODS

In this chapter, the process of selecting the suitable polymer matrix, neutron absorber and solvent based on the study of the literature review are illustrated. The section describes how the polymer composite of this study was manufactured based on mathematic calculation and the use of the solvent casting method. The supernatant left from the production was also analysed using UV-Vis spectrophotometer. Furthermore, this section will demonstrate the neutron experiment, where the neutron-shielding efficiency of polymer composites with different weight percentages (10, 20 and 30 wt%) of neutron absorber was tested. The part also includes an introduction on the use of neutron source (Am-Be), helium detector and other essential devices for the pulse-height analysis.

3.1 Material Selection

3.1.1 Boric Acid as neutron absorber

In the beginning, the thesis aim was to use lithium because it does not produce high-energy gamma as compared with boron, despite two of its major disadvantages. However, as boron compounds were more well-established than lithium compounds in the literature, it gave the study more ideas on how to introduce the boron compound into the polymer matrix. Due to the limited time frame for the thesis's experiment, the development of lithium compound as a neutron absorber could not be achieved in time. Therefore, boron compound was chosen as the neutron capturer. In comparison, boron does not produce as high-energy gamma-ray as cadmium and gadolinium after the nuclear reaction. A light-weight layer of polymer composite for gamma-shielding can be added in the end to avoid

the drawback of boron reaction. Pavlenko et al. (2019) has established a shield made of polyimide/bismuth oxide (PI/Bi_2O_3) composite for the gamma-shielding purpose with an energy range of 0.1 – 1 MeV. It was reported that the shield not only reinforced the thermal stability of the material but also improved the gamma shielding effectiveness due to the introduction of bismuth element into the PI matrix. For the thesis study, a similar gamma shield can be developed as a second layer to stop gamma energy (0.478 MeV) from the neutron-boron nuclear reaction.

It had been reported by Soltani et al. (2016) and Shin et al. (2014) that B_4C and BN showed an outstanding impact on the material behaviour. The two compounds have an effective reinforcement on the mechanical and thermal properties of polymer composites. Hence, it was desired to study B_4C or BN as neutron capturer in PEI matrix in the beginning. However, two compounds were found to be extremely costly for the study case. Additional to B_4C and BN, boric acid (H_3BO_3) had been recently studied as a neutron absorber. H_3BO_3 was a good alternative selection for this study. According to Özdemir et al. (2016), H_3BO_3 is a potential active material for neutron shielding application. It is widely used as a neutron poison in reactors of the nuclear industry. Furthermore, H_3BO_3 was recorded to be an environmental-friendly, safe, non-polluting, and non-toxic compound, accepted by the Environmental Protection Agency and the Clean Water Act federal law (Özdemir et al. 2016). The introduction of H_3BO_3 into the polymer matrix can lead to an effective neutron absorption material.

However, Özdemir et al. (2016) also reported that the increased content of H_3BO_3 (more than 20 wt%) within EPDM rubber had diminished the composite material's strength. It was thought that H_3BO_3 might not always be the factor that weakens the mechanical strength of the material. As the problem was addressed in section 2.4.2 of the thesis, high-hydrogen content of EPDM rubber can cause the decrease of mechanical and thermal stability. Increasing the content of H_3BO_3 within EPDM matrix is the same as increasing the hydrogen content of the material, leading to mechanical failure despite it enhances the neutron capture capability of the material. On the other hand, having the same amount of H_3BO_3 within PEI matrix can result differently. PEI has a strong mechanical strength because of its low hydrogen-content. This can be a major disadvantage for neutron shielding. Therefore, the introduction of H_3BO_3 can improve this weakness since it increases

hydrogen content as well as introduces boron element into the matrix. H_3BO_3 can be the potential neutron absorbers as compared to boron carbide and boron nitride.

3.1.2 Polyetherimide

The author of this thesis is intrigued to study the aromatic polymers rather than aliphatic polymers. Based on Bate (2009), the beginning plan was to use PI for the thesis's study as well. Therefore, there is one alternative, which is to study the potential of a family of PI – Polyetherimide (PEI). Kiefer (2011) once mentioned in his paper about how PEI can be a good consideration for the use of neutron shielding in space. However, PEI had not been as well-studied as PI. To the best of our knowledge, the use of H_3BO_3 loaded in PEI matrix for neutron shielding application has not been encountered specifically.

In contract to PI, which is a thermoset polymer, PEI is a high-performance thermoplastic with excellent mechanical strength, high thermal-oxidative stability, long-term chemical and temperature resistance. Commercial PEI named Ultem 1000 had been reported to have exceptional flexibility, as compared with PE. As stated by Kiefer (2011), thermoset PI could be neither melted nor dissolved once formed a clear structure. It was thought that the study of thermoplastic polymer PEI for the case would be easier to experiment as a first step. According to McMillan (2009), the usage of thermoset polymers/resins with lithium/boron composite could create difficulty to re-use the material, especially for the field of particle-astrophysics. This restricts the material's applications and leads to an extravagant cost of material's quantities. In this study, PEI was preferable instead of PI, despite having a very low hydrogen content as claimed by Bate (2009). Furthermore, PEI had been reported to be a good solvent-resistant thermoplastic (Johnson & Burlhis 1983), where the polymer demonstrated good resistance to the effect of organic solvents. The thesis desired to study the potential of PEI as a neutron-radiation shielding in the space environment. The repetitive unit of PEI can be illustrated as in Fig. 14.

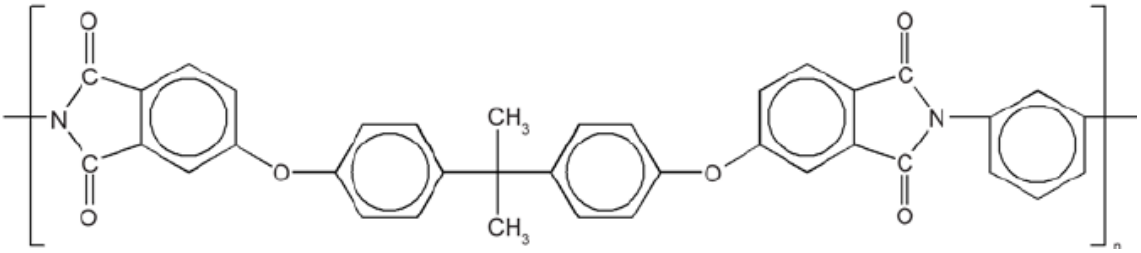

Figure 14. The repetitive unit of polyetherimide (Ultem 1000) (Abbasi, Antunes & Velasco 2015).

3.1.3 Solvent

The solvent is one of the chemicals that played an important role in the thesis's experiment. In this section, the process will describe the selection of diverse potential solvents in dissolving PEI as the first step. Since Ultem 1000 is a slightly polar polymer with functional groups such as ether and amide, PEI might have been soluble in polar solvents.

For the study case, dipolar aprotic solvents are the candidates since they possess several beneficial advantages such as the wide solubility range and the complete miscibility with water. They are strongly utilized for various applications in preparative chemistry, especially in vinyl polymerization process (Reine et al. 2003). According to the research of Rajasekar et al. (2012), dipolar aprotic solvents had effectively dissolved PEI with different chemical groups. In their study, eight structures of PEI had been investigated in many areas, including the solubility in some dipolar solvents. Since the research's sample PEI-3 (see Fig. 15) had had the most similar structure as compared to Ultem 1000, its solubility's table (see Table 1) was taken into consideration as a first step in selecting suitable solvents for the thesis. Six solvents had been tested: Pyridine (C_5H_5N); Chloroform ($CHCl_3$); Sulfuric acid (H_2SO_4); N, N-Dimethylformamide (DMF); Dimethyl sulfoxide (DMSO) and N-Methyl-2-pyrrolidone (NMP) (Rajasekar & Venkatesan 2012).

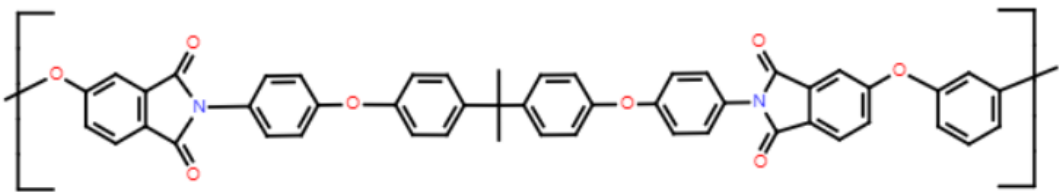

Figure 15. The monomer of PEI-3 in the research (Rajasekar & Venkatesan 2012).

Table 1. The solubility of PEI-3 in selected solvents (DMSO, NMP, DMF, Pyridine, Chloroform and Sulfuric acid (Rajasekar & Venkatesan 2012)

Polymer	DMSO	NMP	DMF	C_5H_5N	$ChCl_3$	H_2SO_4
PEI-3	Soluble	Soluble	Soluble	Soluble	Soluble on heating	Soluble

Since PEI-3 had different structure from Ultem 1000, the process continued to investigate the compatible solvents based on six experimental dipolar solvents from Rajasekar's and Venkatesan's research. The summarized findings are illustrated (see Table 2).

Table 2. The solubility of Ultem 1000 in DMAc, DMF, NMP, DMSO, $ChCl_3$, H_2SO_4 and C_5H_5N

Dipolar aprotic solvents	DMAc	DMF	NMP	DCM	DMSO	$ChCl_3$	H_2SO_4	C_5H_5N
Ultem 1000	+-	++	++	--	--	--	+-	?
++= Soluble; +h = soluble on heating; +- = Partially soluble; -- = insoluble even on heating ? = unknown/no report was found								

Beyond the six solvents represented in table 1, two other solvents: N, N-Dimethylacetamide (DMAc) and Dichloromethane (DCM) were also taken into the study. Having the same advantages, DMAc and DCM acting as the dipolar aprotic solvents are also well-used in dissolving polymers. Additionally, DMAc contains an excessive resolving ability for high molecular-weighted polymers and owns the miscible property that can be widely applied for organic and inorganic compounds. Theoretically, it can also act as intermediate for the synthesized process of some substances (Background document for DMAC 2012). On the other hand, the soluble information of Ultem 1000 in C_5H_5N could not be found, which was not the preferred solvent for the study case.

Scarlet et al. (2012) had studied the solubility of Ultem 1000 in various type of organic solvents (pure solvents or a mixture of solvents). Four solvents: NMP, DCM, DMSO and $ChCl_3$ had been considered. Based on Hansen parameters (2007), the calculations on the interaction of four solvents and PEI had been performed. Results show that NMP had effectively dissolved the structure of Ultem 1000, in contract to DCM, DMSO and $ChCl_3$ (see Table 3).

Table 3. Hansen solubility parameter for individual solvents: NMP, DCM, DMSO and $ChCl_3$ (Scarlet et al. 2012)

Solvents	Ratio	δ_d	δ_p	δ_H	D (R_a)	d_0 (R_0)	Solubility
NMP	-	18	12.3	7.2	5.28	< 6	Soluble
DCM	-	17	7.3	7.1	6.76	> 6	Insoluble
DMSO	7/3	16.58	8.63	8.10	6.20	> 6	Insoluble
$ChCl_3$	-	17.8	3.1	5.7	6.64	> 6	Insoluble

δ_d: energy from dispersion bonds between molecules.
δ_p: energy from the dipolar intermolecular force between molecules.
δ_h: energy from hydrogen bonds between molecules.
D: the experimental radius of solvents.
d_0: The radius of the solubility sphere.

Vora et al. (2005) had further reported about their experiment on the solubility of Ultem 1000 in some organic solvents: DMF, DMSO, NMP, H_2SO_4 and DCM. The solubility of Ultem 1000 can be seen from Table 4.

Table 4. The solubility of Ultem 1000 in DMF, DMSO, NMP and DCM (Vora et al. 2005)

Solvents	DMF	DMSO	NMP	DCM	H_2SO_4
Ultem 1000	+	-	+	-	+-

++= Soluble; +h = soluble on heating; +- = Partially soluble; -- = insoluble even on heating

The solubility of Ultem 1000 in DMAc solvent had been tested by Mills (2010) in her master's thesis. As the results, Ultem 1000 had been partially dissolved in DMAc solvent (see Fig. 16). Therefore, DMAc has been widely applied in creating a polymer composite for neutron shielding and showed great efficiency in dissolving polymers. It was considered that DMAc might have the potential for the study case.

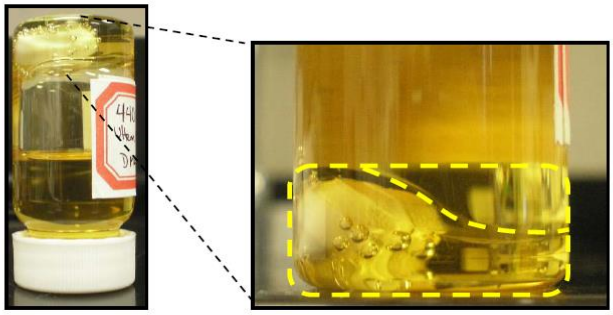

Figure 16. Mill's experiment had shown Ultem 1000 partially dissolve in DMAc solvent (Mills 2010).

Generally, DMF, NMP, H_2SO_4 and DMAc were theoretically studied to dissolve Ultem 1000. Among the four solvents, DMF solvents were purchased by Arcada University of Applied Sciences for another research. Since the experiment of producing the shielding composite was performed at Arcada's Chemistry Laboratory, DMF solvent was firstly used to test the solubility of PEI and H_3BO_3.

3.2 Materials

The neutron-shielding potential of PEI/H_3BO_3 composite was studied in this thesis. PEI which was donated by SABIC with the commercial name Ultem 1000 had the form of transparent amber resin. H_3BO_3 was purchased from Sigma-Aldrich with a minimum purity of 99.8%. Table 5 reported a small percentage of some mixed elements in the H_3BO_3 product. For the solvent casting experiment, DMF solvent, which was also from Sigma-Aldrich with minimum 99.5% of purity. There were some mixed contents in the DMF solvent as well (see Table 6).

Table 5. Content of H_3BO_3 compound

Material	Amount (%)
Chloride (Cl)	Max 0.0003
Sulphate (SO_4)	0.0005
Phosphate (PO_4)	0.0005
Lead (Pb)	0.0005
Iron (Fe)	0.0001
Arsenic (As)	0.00005
Magnesium (Mg)	0.0005
Calcium (Ca)	0.002

Table 6. Content of DMF solvent

Material	Amount
Acidity	Maximum 0.0005 $\frac{meq}{g}$
Alkalinity	Maximum 0.0002 $\frac{meq}{g}$
Heavy metals	Maximum 0.0002 %
Residue	Maximum 0.001 %
Water	Maximum 0.1 %

3.3 The manufacture of PEI/H_3BO_3 composite

3.3.1 Plan

In the beginning, the synthesis plan of the thesis study was based on Li et al. (2018). The intention was to synthesize PEI from scratch using P-phenylenediamine (PPD) and 4,4'–bisphenol A dianhydride (BPADA). H_3BO_3 will then be introduced in the solution, mixed slowly and applied the thermal heating process to create a composite of BPADA/PPD/H_3BO_3. Unfortunately, the polymerization of PEI from scratch was too complicated and time-consuming for this thesis in the beginning. The plan was to use the commercial PEI resin instead. The solvent casting method was still applied to create a homogenous distribution from PEI resin and H_3BO_3. The solubility of two matrixes was tested in DMF solvent. Once achieving a final compatible solution, the H_3BO_3 was introduced in the dissolved mixture of PEI with the desired amount. The solution was stirred until the additive appears to be dispersed. It was then naturally dried in room temperature for solvent evaporation. Since there will be no polymerization taking place, the thermal-imidization heating process was inessential for the study case. In the end, the PEI/H_3BO_3 can be achieved. Fig. 17 below describes the procedure of the thesis experiment.

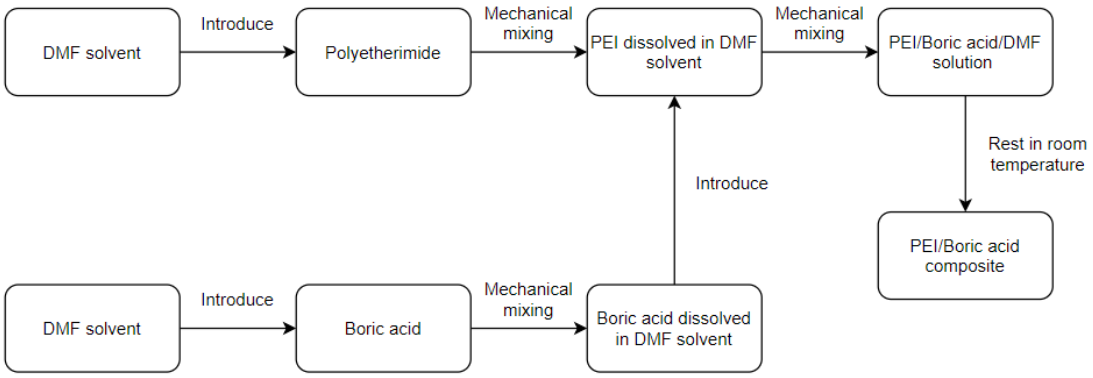

Figure 17: The flow diagram illustrates the experimental method of the thesis (2019).

3.3.2 Solubility tests

The experiments were made to observe whether PEI could be dissolved completely in DMF solvent. Moreover, the solubility of neutron absorbers (H_3BO_3) was tested in the use of DMF solvent for the solvent casting experiment.

The solubility of Ultem 1000 in DMF solvent was experimented in the fume cabinet. 3 ml of DMF solvent was introduced with a micropipette into the test tube which contained a small portion of PEI (0.18 g). The tube was closed by a stopper, shaken well and rested overnight at room temperature. At first, it was observed that Ultem 1000 did not dissolve. The solution was then rested at room temperature for five days. In the end, Ultem 1000 was recorded to dissolve completely in DMF solvent.

The solubility of H_3BO_3 in DMF solvent was tested in the fume cabinet. The experiment was conducted with the same process: 3 ml of DMF solvent was introduced into the test tube containing 0.21 g of H_3BO_3. The test tube was closed by a stopper and shaken for 30 seconds. The reaction showed result quickly after a few minutes. It was observed that H_3BO_3 was dissolved successfully in DMF solvent on the same day.

3.3.3 Material Quantity Calculation

The PEI/H_3BO_3 composite should obtain a certain shape that minimizes the use of pristine materials and maximize the neutron-shielding performance of the material. Since the helium detector has a diameter of 25.5 mm, the composite should achieve a cylinder shape with a diameter of $\geq$ 25.5 mm (ignoring the thickness). From the known information, the demanded quantity of raw materials could be calculated. According to Collins (2015),

a sample with an areal density of $1\,\frac{\mathrm{g}}{\mathrm{cm}^2}$ is recommended for neutron testing. By using the cylinder's base area and density formula, the total minimum mass demanded the thesis's experiment can be known. The base area of the cylinder is expressed through Eq. (3.3.3.1), where r is the radius of the composite

$$\mathrm{A_B} = \pi \times \mathrm{r}^2 \tag{3.3.3.1}$$

To achieve the theory areal density for the shielding material, a random diameter of the composite was assumed for anticipating the mass of each constituent of the composite. 30 mm was assumed to be the composite's diameter ($d_{composite} = 30\,mm = 0.03\,m$), the area will then be

$$\mathrm{A_B} = \pi \times \left(\frac{\mathrm{d_{composite}}}{2}\right)^2 = \pi \times \left(\frac{0.03}{2}\right)^2 \mathrm{m}^2 \;\approx\; 7 \times 10^{-4}\,\mathrm{m}^2$$

From the unit scale, Eq. (3.3.3.2) describes the equation of areal density

$$\mathrm{d\ (areal\ density} - \frac{\mathrm{kg}}{\mathrm{m}^2}) = \frac{\mathrm{m\ (mass - kg)}}{\mathrm{A_B\ (area\ of\ the\ composite - m^2)}} \tag{3.3.3.2}$$

Since the recommended areal density of the material is $1\,\frac{g}{cm^2} = 10\,\frac{kg}{m^2}$, the total mass of the PEI/H_3BO_3 composite was:

$$\mathrm{m_{composite}} = \mathrm{d} \times \mathrm{A_B} = 10\,\frac{\mathrm{kg}}{\mathrm{m}^2} \times 7 \times 10^{-4}\,\mathrm{m}^2 = 7 \times 10^{-3}\,\mathrm{kg} = 7\,\mathrm{g}$$

3.3.4 Solvent cast PEI/H_3BO_3 composite

PEI was used as a matrix for the synthesis of composite in the form of resin. Three PEI samples regarding the weight percentage were prepared. Three samples were dried at 140℃ for 4 hours using a dryer (LABOTEK 101138) before the experimental use. All samples were then dissolved separately in 30 ml DMF solvent in a reagent bottle with a mechanical stirrer at room temperature for four days. H_3BO_3 was introduced as a neutron-captured filler into the PEI's matrix. Three samples of H_3BO_3 were prepared with the desired weight percentages. The acids were dispersed separately in DMF solvent with ratio 7:30 in a test tube. H_3BO_3 dissolved immediately after a few times mixing. The dissolved H_3BO_3 was introduced into the dissolved PEI with appropriate mass (following the desired wt%) and mechanically mixed on the magnetic stirrer. The solution was then

continuously stirred until the homogeneous dispersion of the composite structure and precipitation process appear. The solid precipitate was then immediately cast into a beaker with 35 mm diameter while the remaining suspension was placed in the reagent bottle for further investigation. The composite of PEI/H_3BO_3 was rested at room temperature for five days until the leftover solvent evaporates completely. The PEI/H_3BO_3 composite films with different filler contents (10, 20, 30 wt%) were achieved.

3.4 Method of UV-Visible spectrophotometer

According to the DMF material safety data sheet (MSDS) (MERCK 2009), the solvent is an extremely toxic and flammable chemical that is harmful to the skin and the respiratory system. It is recommended that heating should not be applied to the DMF solvent. Reportedly, its flashpoint is 57.5℃ which is critical to heat the solvent above the safe zone ranging from 43℃ to 57.5℃. Above the recommended temperature can cause fire and other hazards. Based on the MSDS, the heating technique to accelerate the evaporation process of DMF solvent should be avoided. Moreover, the vapour of DMF solvent caused by heating can contaminate the environment. This goes the same when using the vacuum pump. The evaporated gas of DMF is toxic and can damage the pure system of the pump. Therefore, two common methods to accelerate the solvent evaporation process were not done in this study.

Unlike other solvents which can be heated or vacuumed, DMF solvent must be rested and dried naturally under the room temperature. In this study, this was a time-consuming process since it could take days or even weeks for the solvent to completely evaporate. A solution was suggested, which was to use the UV-Vis spectroscopy to analyse the supernate liquid resulted from the phase separation of PEI/H_3BO_3/DMF solution. When the solution of H_3BO_3/DMF was introduced into the PEI/DMF solution, the process formed precipitation, creating a phase separation where the precipitate was rested at the bottom and the supernatant was on the top after the mechanical process of mixing. It was assumed that the precipitate was PEI/H_3BO_3 composite while the supernate was only DMF solvent. However, this hypothesis was unsure since the supernate might be the suspension of DMF solvent containing some H_3BO_3 particles (or even with PEI particles) that was not homogeneously distributed within the incorporated matrix. Moreover, UV-Vis method was also used to determine the experimental wt% of PEI and H_3BO_3 after the production process.

This study showed if the desired wt% of each constituent was successfully achieved. Fig. 18 is the phase separation of PEI/H_3BO_3/DMF solution.

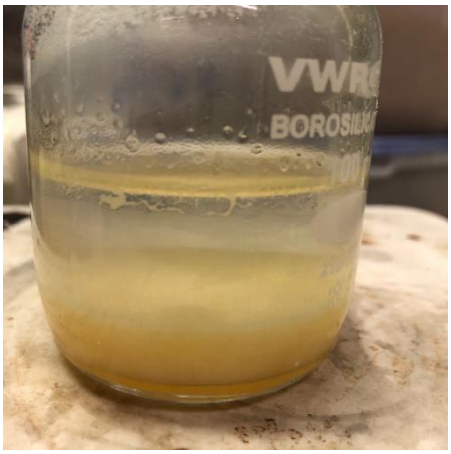

Figure 18. The production of solvent casting technique (2020).

The characteristic of the suspension could be identified using the UV-Vis spectroscopy. The goal of the experiment was to determine the inorganic (H_3BO_3 or PEI) concentration exited in the supernatant of PEI/H_3BO_3/DMF solution through this quantitative method. The supernate could be disposed if no concentration was found. The plan started with the measurement of the H_3BO_3 concentration in the supernate solution first. For the experimental comparison, a set of random concentration of H_3BO_3 in DMF was made (see Table 7). The idea was to measure their absorption based on the reference sample of pure DMF, then compare those data with the supernatant's absorption. Since the beginning assumption was that the supernatant was the DMF solvent containing some H_3BO_3 particles only (ignore the presence of PEI particles), the concentration of H_3BO_3 particles existed in the supernatant could be determined through its experimental absorption, comparing to the data of the random H_3BO_3.

Table 7. Studied H_3BO_3 concentrations in DMF solvent

Sample	Mass of H_3BO_3 (g)	Volume of DMF solvent (ml)	Concentration ($\frac{g}{ml}$)
1	0.1	2	0.05
2	0.1	1	0.1
3	0.3	2	0.15
4	0.2	1	0.2

The UV-Vis (JASCO V-670) instrument was used for the experiment. The software used for the analysis was Spectra-Manager (see Fig. 19).

Figure 19. JASCO V-670 UV-Visible Spectrophotometer and Spectra-Manager software (2020).

The experiment was carried out across the wavelength range from 400 nm to 850 nm at a scanning speed of 1000 $\frac{nm}{min}$. The spectrophotometer analysed the absorption spectrum of the studied H_3BO_3 concentrations in DMF, based on the reference cuvette data which contains only DMF solvent. The result showed that there was no significant absorption value of H_3BO_3 concentrations which could be detected in the visible spectrum. The scanning wavelength was changed to the spectrum of ultraviolet (250 nm to 395 nm) at the speed of 100 $\frac{nm}{min}$. The spectrum of the studied H_3BO_3 concentrations in DMF were recorded. The supernate was then placed in the sample cuvette to analyze its absorption spectrum in this range.

The data showed that the supernatant contained not only H_3BO_3, but also some PEI particles as well. The next idea was to measure the absorption of PEI/DMF solution with the concentration of 0.1 ($\frac{\mathrm{g}}{\mathrm{ml}}$) and compare its data to the supernatant. The same ultraviolet spectrum (250 nm to 395 nm) with a speed of 100 $\frac{\mathrm{nm}}{\mathrm{min}}$ was used for this experiment.

3.5 Neutron experiment

Due to the Corona pandemic, the neutron study could not be completed directly by the author. The processes of experimenting the neutron shielding potential of composites

were performed by the author's supervisor – Erik Brücken at the Helsinki Institute of Physics which is operated by University of Helsinki.

3.5.1 Americium-241/Beryllium neutron source

In this thesis, the neutron source – Americium-241/Beryllium – was used to test the neutron-protective characteristic of PEI/H_3BO_3 composite. Americium-241 is a common isotope of americium with a half-life of 432.2 years. The operation of this neutron source is based on the radioactive decay of Americium-241. Being an unstable isotope, alpha particles, americium's daughter nuclide and an amount of gamma energy of 5.638 MeV are emitted. The reaction was described by L'Annunziata (2016) as below:

$$^{241}_{95}Am \rightarrow {}^{237}_{93}Np + {}^{4}_{2}\alpha^{+2} + \gamma\ (5.638\ MeV) \qquad (3.5.1.1)$$

After the decay process, americium acts as the alpha source where it reacts with beryllium to produce neutron particles. The working principle of the Americium-241/Beryllium neutron source is expressed through the reaction:

$$^{4}_{2}\alpha^{+2} + {}^{9}_{4}Be \rightarrow\ {}^{12}_{6}C + {}^{1}_{0}n + \gamma\ (5.71\ MeV) \qquad (3.5.1.2)$$

In this study, the Am-Be source emits neutrons which have a wide range of fast energies (see Fig. 20). This is also the neutron source's disadvantage since the neutron energies are not uniform and monoenergetic. In the end, one could not determine exactly the amount of neutron energy (MeV) that interacted with the detector. However, the incoming fast neutron (above 1 MeV) could be counted.

The fast neutron energies versus the relative intensities were measured at AEA technology QSA using a stilbene crystal and pulse shape discrimination. The spectrum was reproduced by courtesy of LORCH, E.A. Moreover, this Am-Be source also emits significant low energy (23% below 1 MeV with mean energy 400 keV).

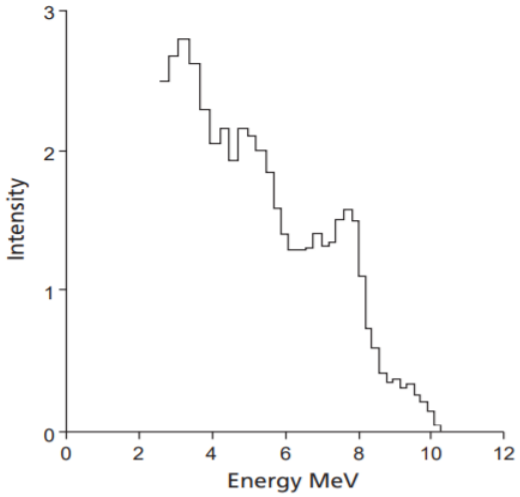

Figure 20. The graph represents the relative intensity-released energy of the Americium-241/Beryllium source (Sealed Radiation Sources 2009).

The neutron cylinder source was doubly encapsulated in welded stainless steel and compacted with a mixture of americium oxides and beryllium metal (Sealed Radiation Sources 2009). In this experiment, the Am-Be neutron source had the capsule type of X.3. The information of the source is displayed in table 8.

Table 8. The information of neutron cylinder source that was used in this study (Sealed Radiation Sources 2009)

Nominal content activity		Emission ($\frac{n}{sec}$)	Capsule type	Code
18.5 GBq	0.5 Ci	1.1×10^6	X.3	AMN.19

3.5.2 Pulse-height analysis

There are various ways to determine the neutron-shielding effectiveness of a composite after its exposure. One can calculate the mass absorption of neutron cross-section of the material or determine the material's attenuation of the neutron permeability ($\frac{I}{I_0}$) versus their thickness or their weight percentage content. In this study, the efficiency of the shielding composite was determined through the pulse-height analysis (PHA), where the number of neutrons was counted and detected before and after the process of shielding.

The helium detector works as a proportional counter – an electrical device that detects the activity of ionizing radiations (beta, alpha, gamma, and neutron) (Proportional counter n.d.). Based on the Townsend Avalanche phenomenon, the detector detects the electronic

pulses which are produced from a single ionizing event after the interaction between the radiation and helium particles (Geiger–Müller tube 2019). The voltage pulses are then collected and converted to form a pulse-height energy spectrum which displays the number of events that are observed and counted versus their amplitude. The PHA is made to examine the voltage amplitude interval of the input pulse (Pulse-Height Spectrometry 2016). In PHA mode, the sum of all electronic pulses is sorted into distinctive memory locations (channels) following their amplitude (Mann et al. 1980, p.197). The lower the total count, the better the shielding potential.

3.5.3 Devices for neutron analysis

To collect, measure and analyse the voltage pulses, various electronic devices were required besides the neutron detector, including the oscilloscope, voltage supplier, multichannel analyser, preamplifier and shaping amplifier.

To understand the system, the full process of the pulse-height analysis was illustrated by Amptek company as seen in Fig. 21. In this study, the test follows this system to perform the neutron pulse-height analysis.

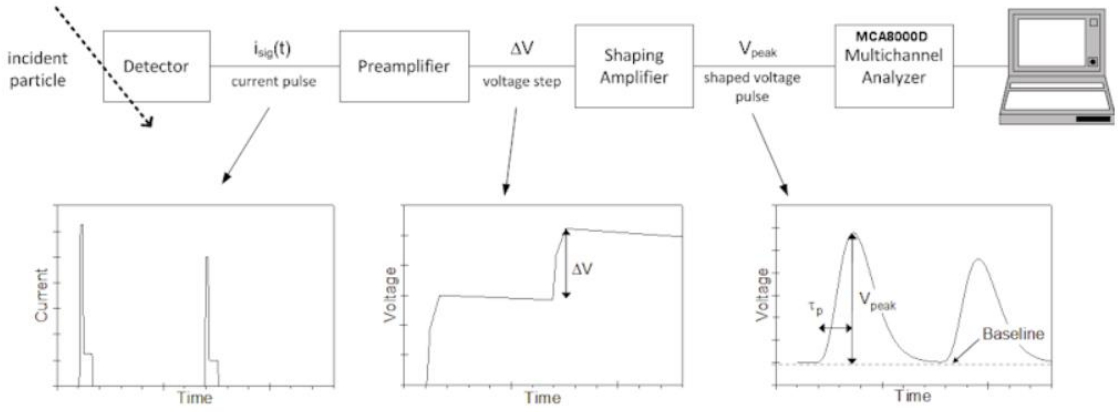

Figure 21. A schematic diagram illustrates the complete pulse-height analysis system (Digital Multichannel Analyzer, n.d.).

The process of collecting and analysing the electronic pulses can be simply explained through Fig. 21. The electronic pulses that are produced from the ionizing events were detected firstly by the helium tube. The preamplifier receives the current pulses from the detector and generates the output voltage pulses with narrow spectrum. This creates difficulties in observing and measuring those data due to the sharp shape of the pulse. The shaping amplifier is used to obtain the signals from the preamplifier and to convert them

into a round spectrum, which is easier for the measurement and analysis. These measurable pulses have the amplitude which is proportional to the neutron energy. The pulse-height distribution can be detected and used as a fingerprint in identifying and quantifying the neutrons and their energies (El-Batanouny 2020, p.190). Finally, the MCA will receive the signal of the voltage pulses from the shaping amplifier and convert the data into digital form, providing the pulse-height spectrometry of the experiment.

Helium detector

The neutron detector is an important device to detect the neutron pulses before and after the process of shielding. For this study, the detector, which was purchased from LND, INC, is a helium detector (25229). The detector has a diameter of 25.4 mm with the effective length of 304.8 mm, an operating voltage range of 900 – 1150 V and a thermal neutron sensitivity of 68 CPS/NV. A mechanical drawing of this helium detector was illustrated by LND, INC through Fig. 22.

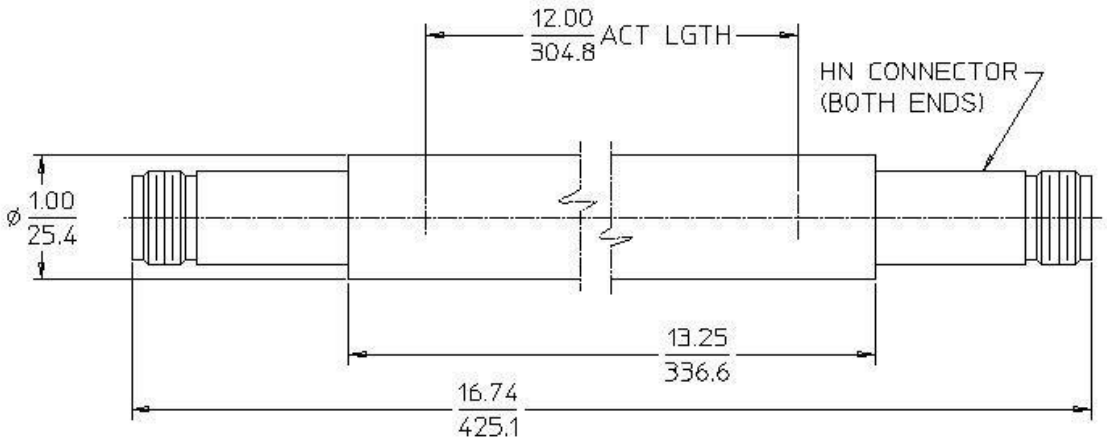

Figure 22. The mechanical drawing of the helium detector on the right-side.

Preamplifier

When using the neutron detector, the signal produced and detected from the helium tube will have very low-level amplitude. To amplify the weak signal to the stronger output signal, charge sensitive preamplifier (CSP) is used. CSP is an electronic device which is capable of integrating the current signal and producing a voltage signal at an amplitude proportional to the input charge (Charge Sensitive Preamplifier 2017). In the study case, a preamplifier (142IH) was purchased from AMETEK-ORTEC. Fig. 23 is a picture of the preamplifier from ORTEC.

Figure 23. The preamplifier (142IH Preamplifier n.d.).

Oscillator, voltage supplier and shaping amplifier

Fig. 24 is a picture of the oscillator, voltage supplier and shaping amplifier that will be used in the test. In this experiment, a digital phosphor oscillator (DPO 3052, 500 MHz) which was purchased from Tektronix was used to set up the measurement. Its mission was to capture the signals from transient events which happened in the helium detector. In other words, it was utilized as the detector's monitoring device. Below the oscillator, a crate was used as the power supply for two devices inside: the shaping amplifier (855 Dual-Spec Amp) which was also from AMETEK-ORTEC was placed on the left and the high voltage power supply (ISEG NHQ 246L) which can deliver up to 6000 V with maximum current 1mA was on the right. In this study, the input voltage for the experiment was 1260 V. The high voltage was connected to the preamplifier.

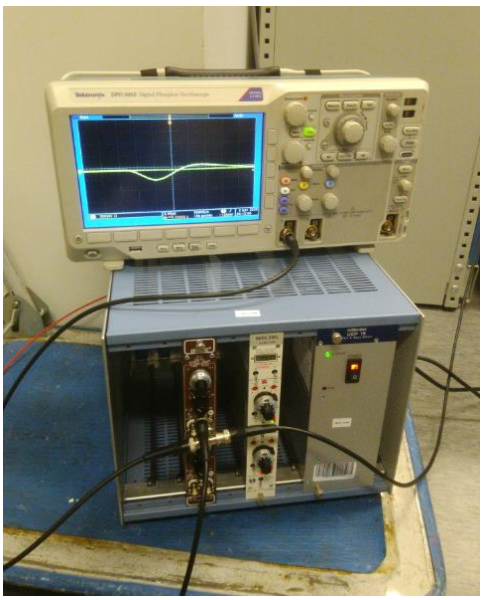

Figure 24. DPO was placed above the crate, which supplies power for the shaping amplifier (on the left) and high voltage power supply (on the right) (2020).

Multichannel analyser

A digital multichannel analyser (MCA-8000D) which was purchased from Amptek was applied to measure the pulse-height spectrum achieved from the shaping amplifier. Its mission was to convert the input signal into a digital form so that the data acquisition can be studied through its software – DPPMCA. The MCA was connected parallel to the oscillator so that the signal could be split to MCA and oscillator. Fig. 25 is the picture of the multichannel analyser and the on-going neutron measurement process, illustrated by DPPMCA software.

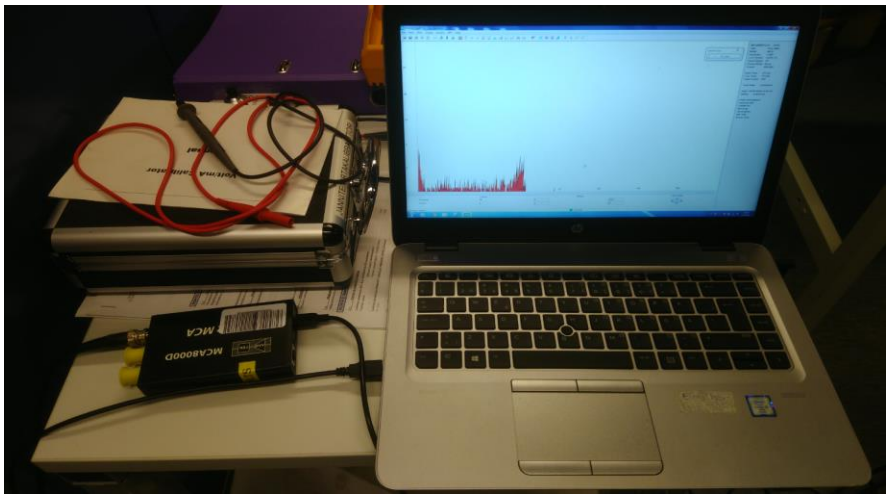

Figure 25. The multichannel analysis was placed on the left and its software (2020).

The incoming neutrons were counted based on their interaction with helium gas particles. In the pulse-height spectrum, the number of events (counts) was demonstrated on the y-axis while the x-axis is the channels. An important property of the MCA was that it measures the amplitude of the electron pulse produced by the single ionizing event and sorts them into the channel with the desired amplitude. In this study, 1024 channels of MCA represented an input voltage range of pulse amplitude from 0 to 1 V. Each channel collected all events that generate the signals of a certain amplitude. For example, channel A (in the range from channel 0th to channel 1024th) measures an amplitude of A/1024 V, collects all events that generate the signal amplitude of A/1024 V and sorts them into channel A.

3.5.4 The steps of neutron test

The results of counting neutrons determined the shielding effectiveness of the composite samples. The lower the count, the better the shield. This experiment was done by comparing the data with the neutron count without the shielding material to know the amount of neutron that can be detected by the helium tube. If the count of shielding materials is smaller than without shielding material, it means that the PEI/H_3BO_3 composite has the potential of shielding fast energy of neutron radiation that usually encounters in the space environment. In the end, the background test was measured to count the neutrons that already presented in the environment at the location near to the experiment area.

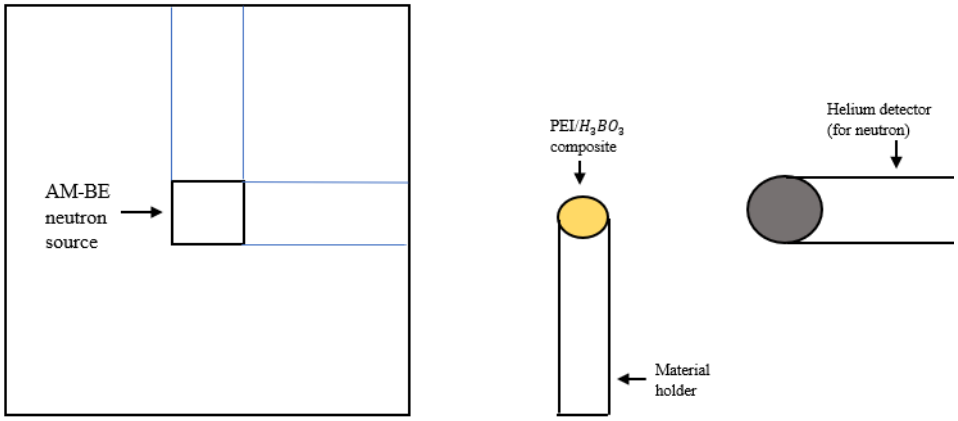

Figure 26. Neutron experimental setup (2020).

Fig. 26 describes the experiment setup. The shielding materials with different wt% of H_3BO_3 (10, 20 and 30 wt%) were tested step-by-step after the measurement of neutron count without the shielding composite. The composites were placed in between the neutron source and the helium detector. Afterwards, the final step was to measure the background/noise. In the end, the pulse-height spectrums of the shielding composites were extracted by the background spectrum. All the tests were measured for 10 minutes (600 seconds). Fig. 27 below is a picture of the neutron experiment.

Figure 27. Top-view of the neutron experiment (on the left) shows the detector and the preamplifier. Side-view of the experiment (on the right) shows the neutron source and other devices (2020).

4 RESULTS

4.1 The result of the solvent casting experiment

Three PEI/H_3BO_3 composites with 10, 20 and 30 wt% of H_3BO_3 (see Fig. 28) were created. Since the tests were performed by hand, the materials were moulded differently, causing the change in shape, thickness, and uneven surface.

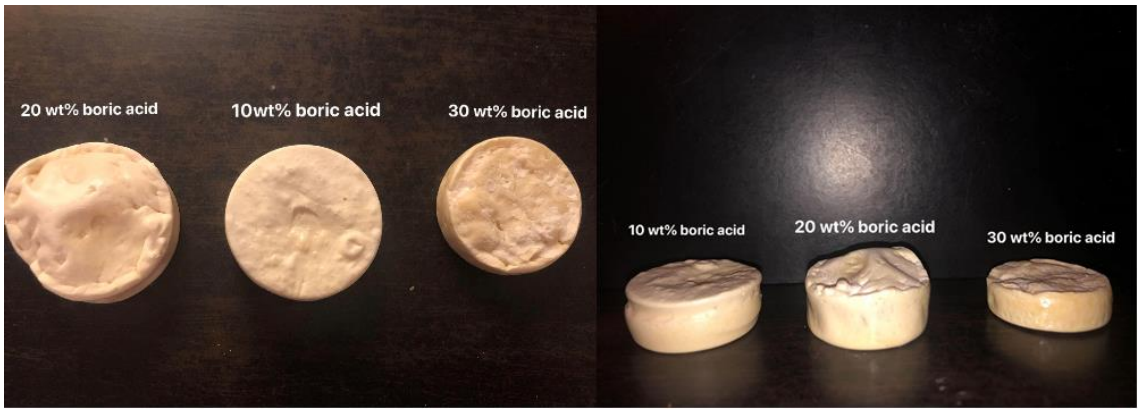

Figure 28. Top-view and right-view of three PEI/H_3BO_3 composites in the second solvent-casting experiment (2020).

The measurements of these three materials are illustrated in table 9.

Table 9. The mass, thickness and diameter of three composites (2020)

	Mass (g)	Thickness (mm)	Diameter (mm)
10 wt% H_3BO_3	11.54	15.5 (average thickness depending on the spot)	35
20 wt% H_3BO_3	12.18	14.5 (depending on the measurement spot)	35
30 wt% H_3BO_3	9.34	10	35

4.2 The result of the UV-Vis analysis

Fig. 29 and Fig. 31 demonstrate the data obtained from the UV-Vis experiment. The first figure showed the absorption of the studied H_3BO_3 concentration in DMF solvent at a specific wavelength of 265 nm. The absorption values (%) of each sample were reported orderly following Fig. 29 (from up to down): 0; 0.27; 0.47; 0.731 and 0.737. Based on the measurement, a linear graph of absorbance regarding the concentrations was made (see Fig. 30).

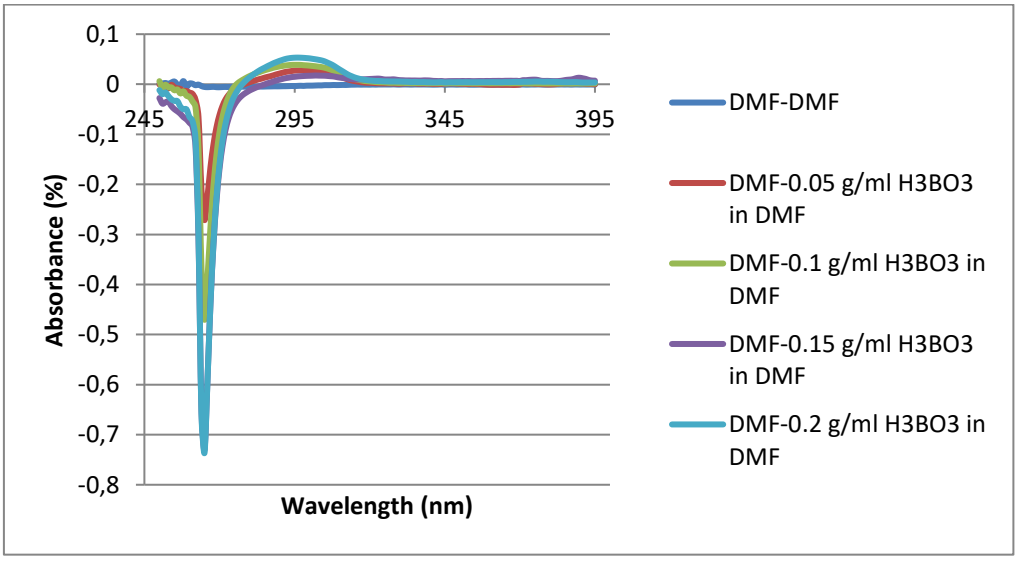

Figure 29. The absorbance of studied H_3BO_3 concentrations in DMF (2020).

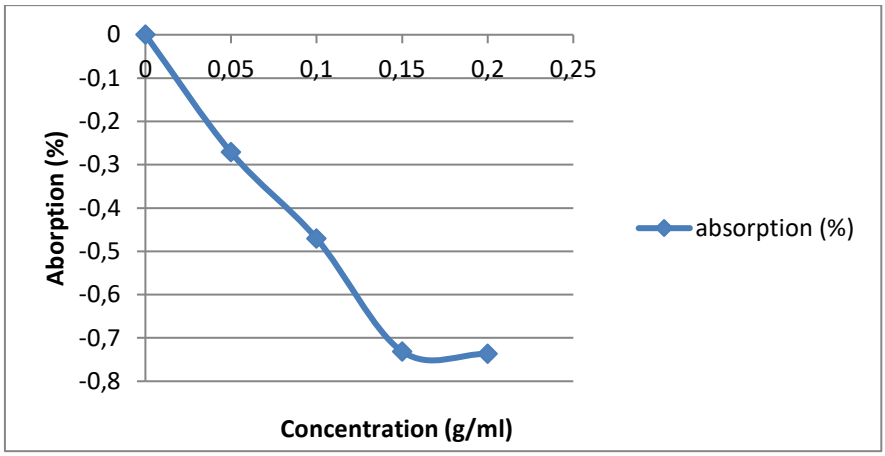

Figure 30. The absorbance-concentration relationship of the studied H_3BO_3 (2020).

According to the plan, the supernatant had been assumed to be some H_3BO_3 concentration in DMF solvent and its absorption should be observed in the range of -1 to 1 (fulfil the Beer's Law requirement). By this way, the concentration of H_3BO_3 existed in the supernatants could be determined through the absorbance. However, all three supernatants were recorded to have much higher absorption than 7. Regarding the reference sample, the solutions contained some other impurities as well, rather than only H_3BO_3 particles. This meant some concentration of PEI particles also existed in the supernatants. To confirm the case, the absorbance of random concentration of 0.1 g/ml PEI dissolved in DMF solvent was measured. Fig. 31 illustrates the absorption spectrums of all three supernatants and PEI concentration in DMF, with the reference sample of pure DMF.

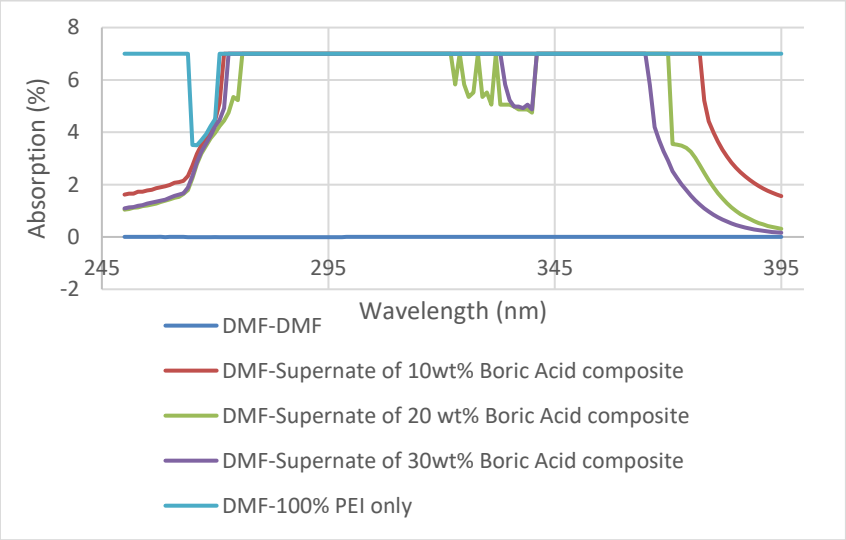

Figure 31: The absorbance of all three supernate solutions and PEI/DMF solution, compared to the reference pure DMF solvent (2020).

4.3 The results of the pulse-height analysis

4.3.1 Raw data

In this section, the pulse-height spectrum and the neutron count of each experimental stage are illustrated. This includes the measurement without the shielding composite, with all three wt% H_3BO_3 composites and background measurement. This part provides the raw data of all stages without background/noise subtraction.

Fig. 32 and Fig. 33 are the pulse-height spectrums without shielding material which was measured twice for 600 seconds. The neutron count of the first test was 874 counts and 947 counts for the second test.

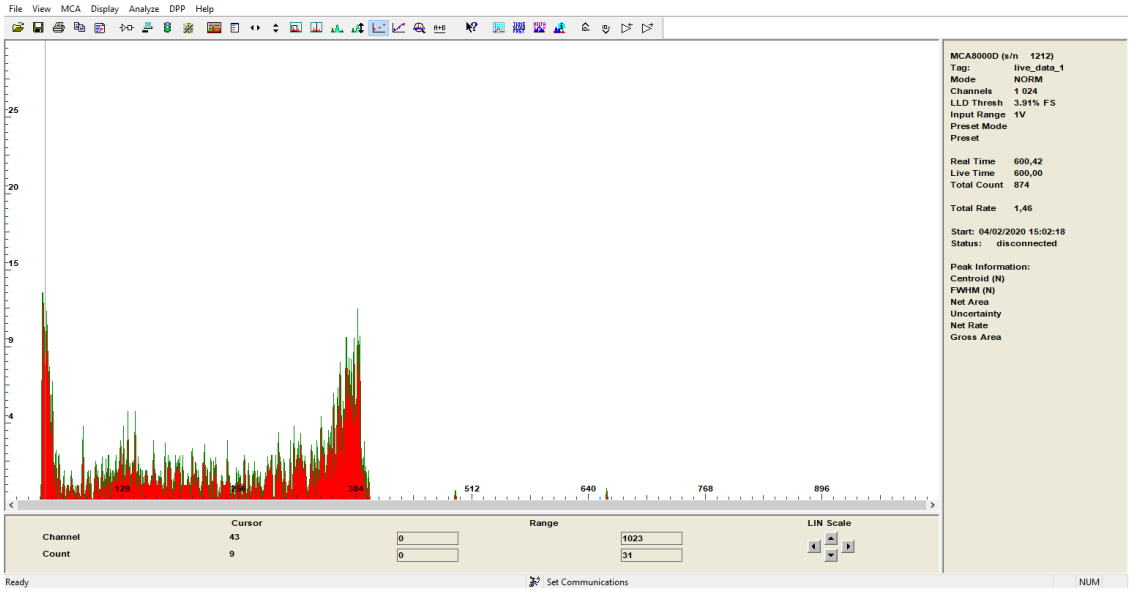

Figure 32. The pulse-height spectrum and the total neutron count without shielding material (1st test) (2020).

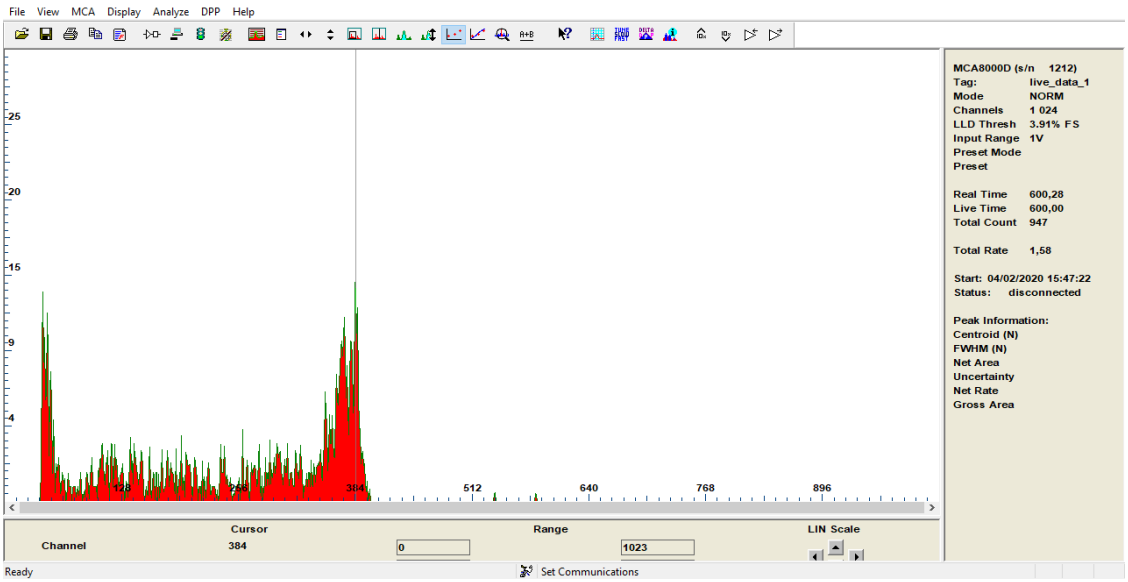

Figure 33. The pulse-height spectrum and the total neutron count without shielding material (2nd test) (2020).

Fig. 34, Fig. 35, and Fig. 36 describe the pulse-height spectrum and the total neutron count of three shielding composites.

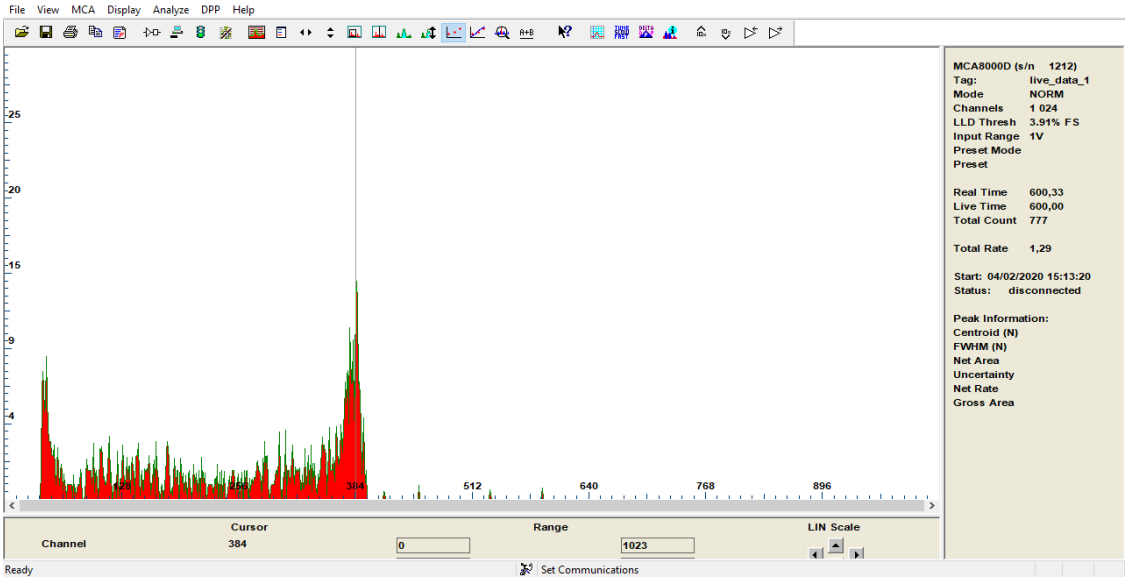

Figure 34. The pulse-height spectrum and the total neutron count of 10 wt% H_3BO_3 sample (2020).

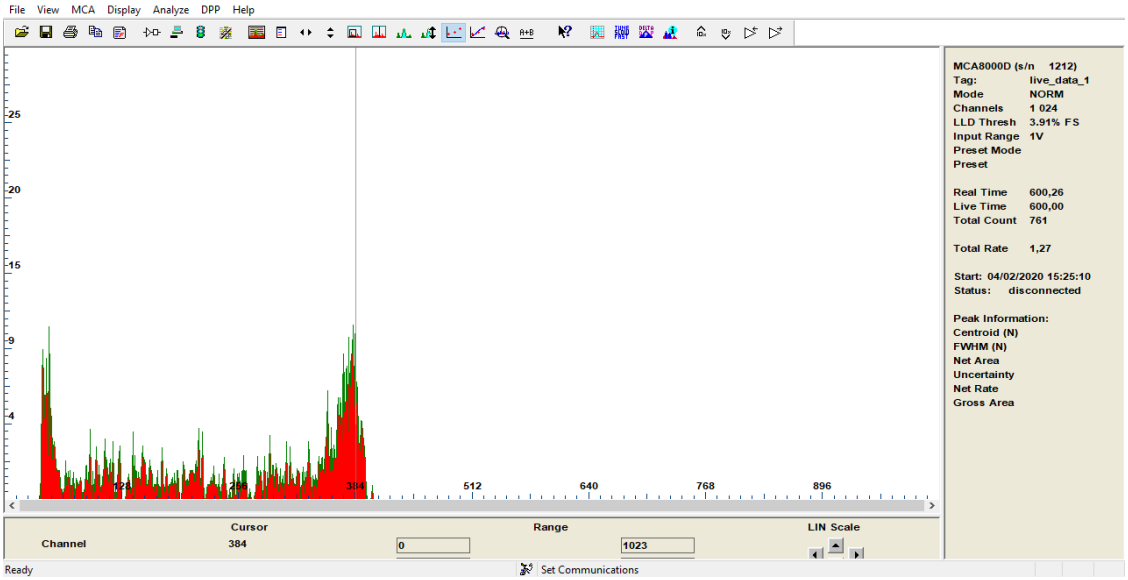

Figure 35. The pulse-height spectrum and the total neutron count of 20 wt% H_3BO_3 sample (2020).

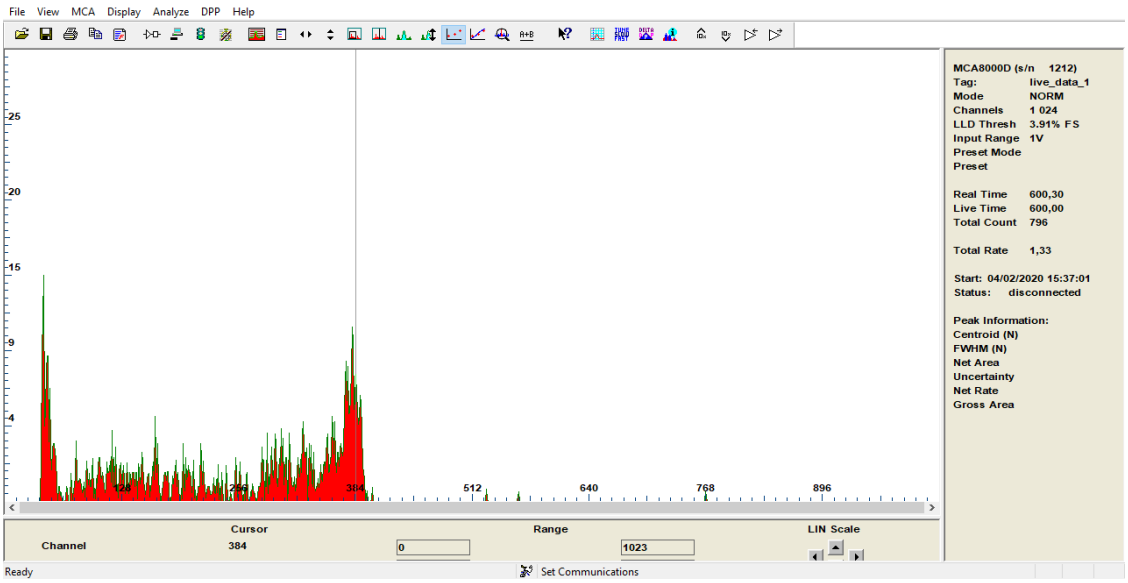

Figure 36. The pulse-height spectrum and the total neutron count of 30 wt% H_3BO_3 sample (2020).

The background test was measured and illustrated through Fig. 37.

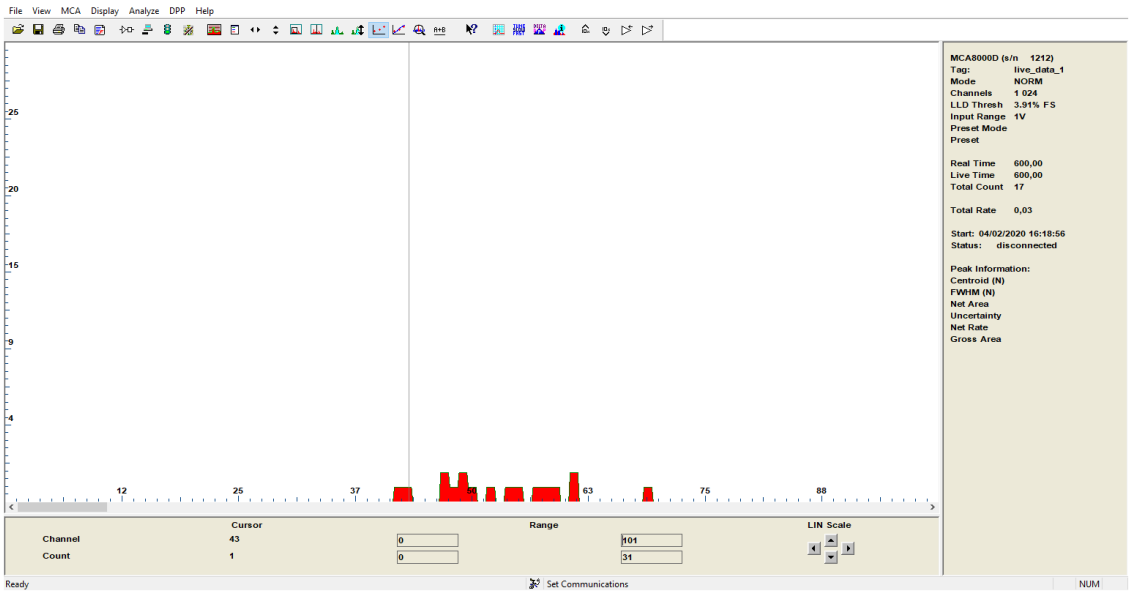

Figure 37. The pulse-height spectrum and the total neutron count of the neutron background test (2020).

4.3.2 Neutron count of each shielding composite after subtracting the background noise

As it can be observed in all the pulse-height spectrums, the neutron count focused mainly from channel 40 to 400 on the x-axis since the further channels which had only 1 count were the result of noise. Moreover, Fig. 35 shows that the background had the spectrum which occurred from channel 40 to 70. The counts that were below channel 70 were the results of background noise. It was assumed that the exponential curve which was from the background spectrum could likely reduce to 0 when it approached channel 70. To remove the noise, Excel was used to re-calculate the total neutron count of each stage with the background subtraction. For two pulse-height spectrums without the shielding composite, the average count was taken into study.

Fig. 38 is the average pulse-height spectrum from the first and second neutron measurement after subtracting the background from channel 40 to channel 70. The total of this spectrum was 767 counts.

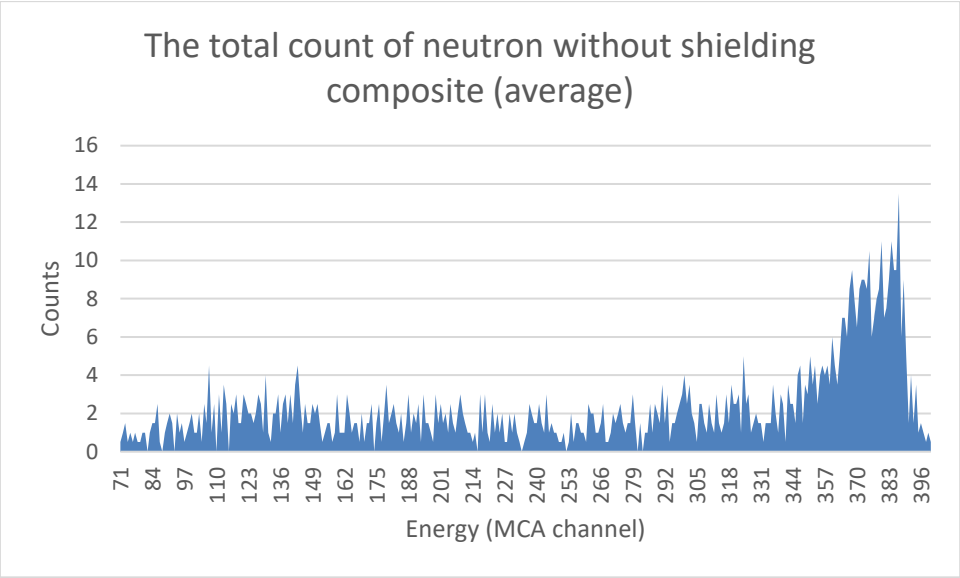

Figure 38. The pulse-height spectrum without shielding material (average from the first and second no sample test), from channel 71 to channel 400 (2020).

Fig. 39, Fig. 40, and Fig. 41 are the pulse-height spectrum of 10 wt%, 20 wt% and 30 wt% H_3BO_3 shielding composite after subtracting the background below channel 70. The total counts were orderly reported: 668 counts, 643 counts and 673 counts.

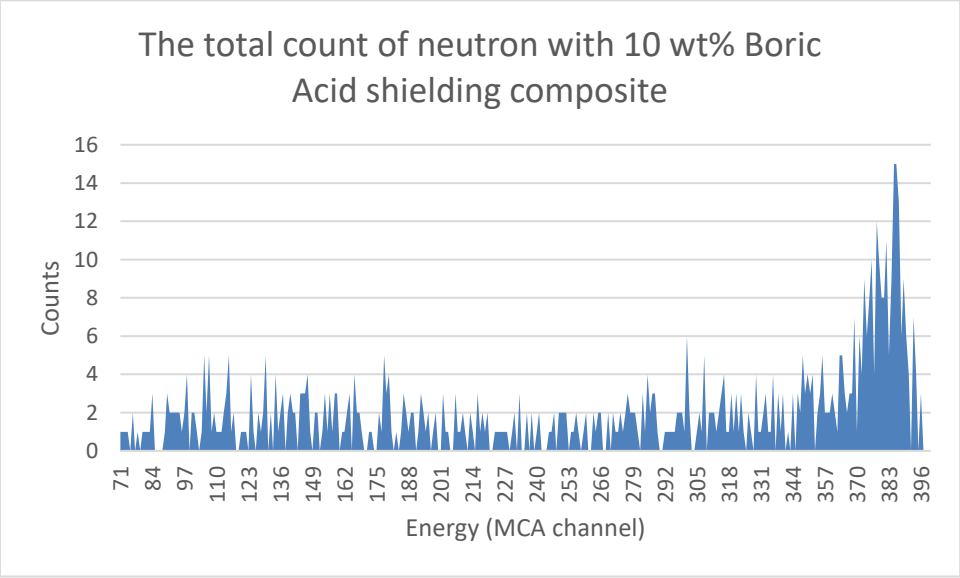

Figure 39. The pulse-height spectrum with 10 wt% H_3BO_3 shielding material from channel 71 to channel 400 (2020).

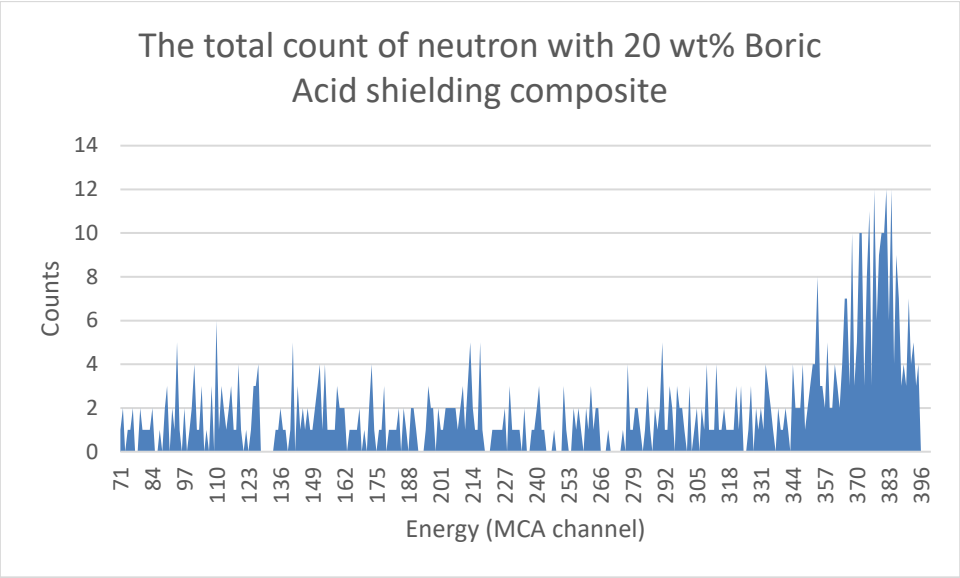

Figure 40. The pulse-height spectrum with 20 wt% H_3BO_3 shielding material from channel 71 to channel 400 (2020).

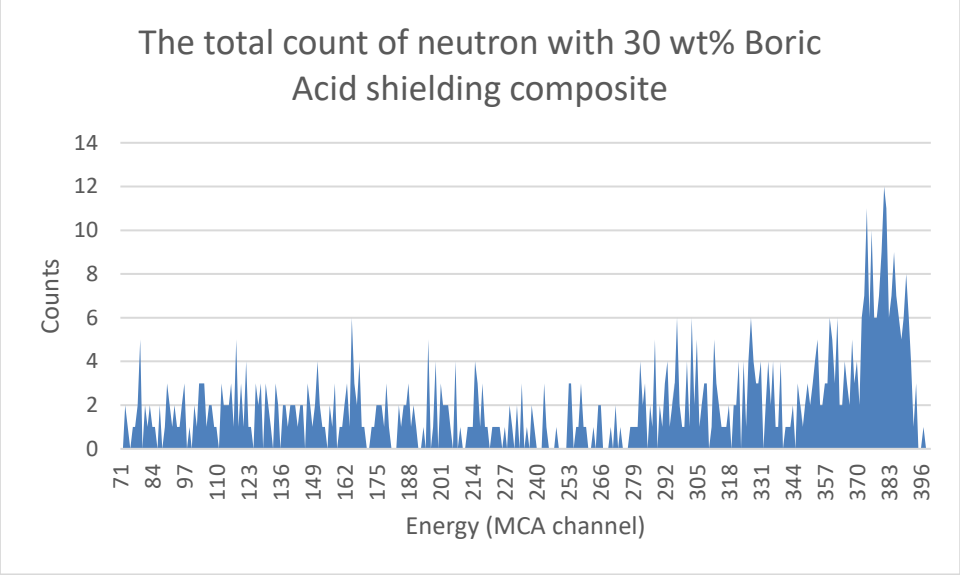

Figure 41. The pulse-height spectrum with 30 wt% H_3BO_3 shielding material from channel 71 to channel 400 (2020).

5 DISCUSSION

5.1 The discussion of the solvent casting composite

The solvent casting experiment created more difficulties in studying the neutron-shielding potential of this composite. Since the uneven surface (especially for the 20 wt% H_3BO_3) gave different thicknesses at different spots of the material, the amount of neutron detection could also vary, giving inaccurate results. As the 20 wt% H_3BO_3 was the thickest, its shielding performance could be the most effective. Furthermore, the experimental mass

of these three composites was much bigger than the theoretical calculation. The extra mass was assumed to be the remained solvent, which was trapped within the material after the experiment and the evaporation process. This happened as the tests were performed by hand. An amount of trapped solvent made the material softer and more malleable, which could strongly decrease the material's mechanical strength as well as its neutron-shielding potential. For instance, Fig. 30 shows the unnormal shape of the 20 wt% H_3BO_3 sample.

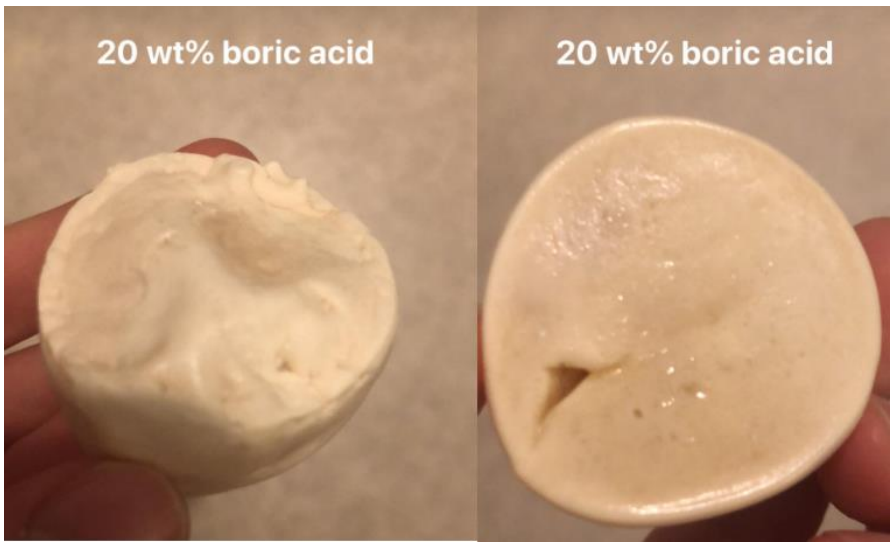

Figure 42. The unusual shape of the 20 wt% H_3BO_3 sample from the second experiment (2020).

Thickness is one of the most important factors that have a strong impact on the shielding effectiveness of the material. Since there was a huge gap between the thickness of the shielding composite, it was invalid to relatively compare the number of neutrons received after each shielding time. Above all, the trapped solvent can also affect the total neutron count. Moreover, the experiment did not obtain the theory of areal density for the material. The material quantity calculation was performed inaccurately due to the selection of random diameter. At that time, 30 mm petri dish could not contain all the material due to its shallow design and there was no replaceable beaker which had a diameter of 30 mm. Therefore, the 35 mm diameter of the beaker was used as an alternative solution. Since the radius affects the areal density of the material, the total mass of each constituent should have been re-calculated, so that the production could obtain the theoretical density for the shielding composite. In general, the experiment did not produce the expect results, therefore, it should be performed again with the correct parameters. Due to the global

pandemic COVID-19, the laboratory experiments were cancelled, and the shielding composite could not be completed in time.

5.2 The discussion of the UV-Vis results

Fig. 31 showed that the chemical reaction from the solvent casting process created a different chemical component in the solution. Two supernatants of 20 wt% and 30 wt% composites were recorded to have spectrums from 323 nm to 339 nm, although there were no spectrums for the concentrations of H_3BO_3 and PEI at these wavelengths. Furthermore, three supernatants did not have a spectrum at the wavelength of 265 nm where H_3BO_3 peak took place but show the PEI curve. It would still be understood that both PEI and H_3BO_3 present in the sample supernatant. As the H_3BO_3 concentration increases, the solubility of PEI in supernatant reduces. Generally, the obtained readings were assumed to be wrong or irrelevant, since their absorptions were much larger than 100 %. The case could also imply that the supernatants contained more impurities than the solution of H_3BO_3 and PEI in DMF solvent, leading to the big difference in the absorption. Moreover, the concentration of 0.1 $\frac{g}{ml}$ of PEI in DMF solvent appeared to have a peak at 265 nm, which happened at the same wavelength as all concentrations of H_3BO_3 in DMF solvent. One assumption was due to the contamination of H_3BO_3 within the PEI/DMF solution.

Through the readings, the supernatants contained much more impurities than the expectation. All supernatants were assumed to be a mixture of DMF solvent, PEI, H_3BO_3 and other compounds which was newly created after the chemical reaction. It was hard to determine accurately and exactly the concentrations of each impurity using the UV-Vis method. The readings were also unreliable and complicated to understand the structure of the compounds existed in the supernatant that causes the spectrum. That is to say, the UV-Vis was not the right method to determine directly and indirectly the concentration of the solution and composite in this case. One could determine the experimental wt% of PEI and H_3BO_3 of the composite using other methods, as compared to the theoretical wt%. This is mentioned in section 5.4.3 of the thesis.

5.3 The discussion of the neutron measurement results

The disadvantage of the experiment was that the fast neutron energy from the source is not mono-energetic, which means its energy could not be determined approximately. In this study, one could not interpret the energy of neutron; therefore, could discuss the kinetic energy of the fission products based on the pulse amplitude. The result of fission is recorded through Eq. (2.7.1), where the total kinetic energy of the daughter products (0.764 MeV) was observed in all measurement stages, starting roughly from channel 370 to channel 400. However, the experimental full-energy spectrum was not sharp as it had been expected in the theory (see Fig. 13), since the full energy was not always absorbed in helium gas. The wall effect could be observed in all the spectrum as well, especially for the 30 wt% sample. To inspect further the effect, one needs to measure the incoming neutrons over a longer time.

In comparison, the spectrum of all shielding materials showed a smaller number of counts and lower count distribution than without the shielding composite, indicating the shielding potential of the composites. Furthermore, when comparing the total neutron count of shielding material to each other, it showed that the 20 wt% sample had the lowest total neutron count while the highest count was obtained by 30 wt% sample. Theoretically, the 30 wt% sample should have obtained the lowest count, as it had the most percentage of neutron absorber. The result could be caused due to the larger thickness of the 20 wt% sample and this issue was anticipated at the beginning of the neutron experiment. The trapped solvent could take part in this result as well. The 10 wt% H_3BO_3sample had the total neutron count in between the 30 wt% and 20% sample, which was understandable since the thickness and the amount of trapped solvent of this composite were larger than 30 wt% sample, but are smaller than 20 wt% sample. That is to say, it was hard to compare the results relative to each other at an unequal parameter.

Furthermore, it was observed that the number of neutrons counted through the process were comparatively low. This could be because of the two paraffin waxes placed in front of the source (Fig. 25) that blocked some incoming neutrons. In the end, it can be concluded that the test's results were invalid and inaccurate since it was performed only once in a short amount of time. The experiment should have been done at least three times to confirm again the number of neutrons detected through three shielding composites at a time and to compare the results between each testing process as well. This helps to

achieve better outcomes with higher accuracy in the shielding potential of the materials. Unfortunately, due to the restriction law for the Corona outbreak, the available time was limited, and the experiment could only be performed once.

5.4 Recommendation

5.4.1 Surface modification

The surface development of polymer composites for the neutron radiation shielding technology has been diversely studied in recent years. It was reported that modifying the surface of inorganic particles can improve the property of final material. There is no doubt that the introduction of inorganic particles into the organic matrix is hard to achieve successfully. The neutron absorber particles might not be able to disperse uniformly and evenly within the matrix, they instead form a cluster of their own. This leads to the decrease of mechanical strength and the ability to capture neutron particles.

According to Pavlenko et al. (2019), the introduction of the inorganic compound into an organic polymer matrix could have resulted in various technical difficulties. Aggregation of the neutron absorber has been one of the factors. In the study case of Pavlenko (2019), Bi_2O_3 was modified to achieve its homogeneous distribution within the polyimide matrix. The modification was obtained using reagents, creating a hydrophobic surface of the inorganic compound. This enhanced the mechanical properties, thermal stability, and neutron absorption capability of the polymer composite. Furthermore, since achieving good, uniform dispersion of the inorganic particles is always the problem, the dispersing agent is another alternation to obtain a better homogeneous structure of final material.

Although various studies reported that modification is a good method to achieve a better property of the material, the influence of H_3BO_3 distribution on the material's neutron shielding ability and the mechanical property was not found in the literature. As a beginner, it was suggested to create the material without modification and dispersing agent first to observe the neutron shielding capability of the material. The result of the test shows whether the material needs either modification or dispersing agent in the end. In the development of a shielding material in space, one should have considered this characteristic result as well. Since the homogeneous factor of the material affects the material

performance, the test of homogeneous surface and mechanical properties should have been carried out to study optimally the potential of the composite.

5.4.2 Scanning Electron Microscopy

As the problem was addressed above, the test on the material's surface is important to maximize the potential of the material. The uniform distribution of inorganic filler should have been observed to carry on the next step. For the study case, Scanning Electron Microscopy (SEM) is suggested to examine the characterization of the material. It is one of the most crucial technics that is frequently applied for the study of polymeric composite in this specific study case. Since the goal is to shield neutron particles, the material is only effective if the inorganic neutron absorber's particles are homogeneously dispersed in the polymer matrix. SEM could show if the experiment successfully achieves the even incorporation between two different constituents of the polymer composite.

5.4.3 The determination of the experimental weight percentage of the composite

Additional to the examination on the homogeneous distribution of the neutron absorber in the PEI matrix, the experimental wt% amount of H_3BO_3 in the composite was expected to have the same amount as in the theory. In the UV-Vis experiment, it was discussed that some concentration of PEI and H_3BO_3 might have not incorporated in the process of forming the composite. This meant that the experimental wt% of PEI and H_3BO_3 of the composite could be lower than the wt% expectation of H_3BO_3 (10, 20 and 30 wt%). A test should be performed on this case using other methods rather than the UV-Vis method. This can help understanding better about the composite behaviour and the differences in their neutron-shielding potential. It is suggested to apply thermal degradation method. Thermalgravimetric analysis (TGA) is one of the instruments that can be used for this measurement. Since the composite's constituents (H_3BO_3 and PEI) have different degradation temperature, TGA provides different slopes based on this feature which corresponds to the weight loss of each constituent. This weight loss is equivalent to the wt% of PEI and H_3BO_3 of the composite after the experiment. However, TGA might not always be an appropriate method to determine accurately the weight percentage of the

neutron absorber. After the solvent casting method, H_3BO_3 could have bonded to PEI and would not present its original structure, which create difficulty for TGA measurement.

5.4.4 Mechanical Tests

The mechanical properties, as well as heat resistance, should have been applied for the study of neutron-shielding material in the space environment. The tensile stress, elongation strain and temperature endurance are important determinants which decide if the polymer composite is good to perform under the harsh space environment. Those factors depend strongly on the homogeneity of the neutron absorber's distribution. The mechanical experiment can be performed using a universal testing machine (UTM). At Arcada, the Testometric M350-5T is one of the options for this test. Moreover, TGA and Differential Scanning Calorimetry (DSC) should also be used to examine the thermal stability, heat resistance and the changing glass transition temperature of the composite. The data obtained from the mechanical test are essential to observe the material performance in normal and space condition. The improvement of mechanical strength of PEI/H_3BO_3 compare as compared to the pristine PEI displays the composite's potential.

5.5 Overall discussion

There were a lot of challenges encountered in the thesis process. Due to the lack of experimental experience, the results of this thesis did not agree with theoretical predictions.. The major issue was with the performance of the solvent casting technique, where the composite thickness was shaped unevenly. This created a lot of difficulties in comparing the shielding efficiency relatively to each composite since thickness impacts strongly on the shielding potential. The calculated mass that was used for the neutron test could not obtain the theoretical areal density, due to the change in the composite's diameter. There was an unknown amount of trapped solvent present in the final composites since the materials were not treated with the right technique. These issues can dramatically decrease the material's potential as well. The plan should have been carried out carefully in the beginning before taking part in the experiment. Although the procedure, example and tips of the solvent casting method have been constantly studied, the results behaved in unexpected ways.

Another issue is the supernatant's compositions after the reaction. Identifying its composition helps not only to decrease the waiting time for the DMF's evaporation, but also indirectly determine the experimental wt% of PEI and H_3BO_3 within the composite, as compared to the desired wt%. Based on the observation, there were some white unidentified particles present in the supernatant after the reaction, thus assuming the supernatant contained only some H_3BO_3 particles in DMF solvent. UV-vis analysis was used to investigate concentrations; however, the presence of significant, unexpected, impurities may have affected the measured results as they deviated significantly from expectations. This technique may not have been appropriate for this purpose. The other methods available at Arcada UAS could also not determine if these particles are H_3BO_3, PEI or new particles born from the reaction. This also leaves an unknown answer about the experimental wt% of each constituent in the composite. There should have been more research on the chemical reaction between the three components (PEI, H_3BO_3 and DMF solvent) to determine the structure of the end products. However, this process was rather complicated to accomplish in a short amount of time.

20 wt% sample showed the lowest count among the three composites as the result of the experimental thickness. For neutron experiment, one should have performed multiple experiments (at least three times) at a longer time for each stage of shielding to confirm the validity and to achieve better results for the thesis aim. There could also have been deeper studies on the neutron experiment to obtain a better understanding, such as the determination of the neutron energy, background subtraction and the full-energy peak. For the background subtraction, the curve of exponential fit which can be obtained from the background should have been applied into the sample spectrum. Having the exponential curve, the actual count of the sample could have been integrated by the subtraction of the exponential area. This provides more accurate count results than only eliminating all counts below channel 70. To perform all these calculations, software such as MATLAB or Python is required, which involves coding skills and mathematical knowledge. This is a complex process that is hard to accomplish without the essential knowledge in a short time. To achieve the best outcome, one should put more effort and time in studying completely the idea. Since the time frame of this thesis was affected by the COVID-19 pandemic, the result could only be interpreted in an simplified way.

Overall, for neutron space shielding application, the desired material is demanded to provide not only neutron shielding potential but also other capabilities such as the heat resistance and mechanical performance to be functional in space. To fully determine the potential of a material, one needs to perform more studies than only neutron shielding aspect. The important factors were emphasized in section 5.4 of this thesis, such as the homogeneous distribution test of the inorganic compound in the polymer matrix, the surface modification test on the material, heat resistance and mechanical capability test. At the beginning of this thesis, it was determined that 30 wt% sample would properly achieve the lowest count. Therefore, it was indeed intrigued to test if the 30 wt% sample would also have acceptable performance in the space environment among all three contents based on mechanical test and thermal decomposition. These main studies on different contents of PEI composite will conclude which content sample have the most optimum properties. Furthermore, the introduction of H_3BO_3 into PEI matrix could not only improve the shielding potential but also enhance the tensile properties, flexibility, and tear strength. In other words, there should have been more characteristic studies on the composite behaviours.

6 CONCLUSION

The objective of this thesis was to develop a new advance polymer composite for the improvement of neutron shielding technology in the space application, rather than applying the traditional shielding materials as before. To obtain a better understanding of radiation generally, and neutron radiation in particular, a literature review about neutron was included. According to the theory of neutron interaction principle and neutron energy in space condition (above the sea level, onboard the ISS and in transit to Mars), multiple data sources were collected and compared on the use of different constituents in producing polymer composite for different types of radiation shielding. Based on the working mechanism of neutron radiation, the thesis described the process of finding and selecting the innovative polymers and neutron absorbers that could provide potential shielding against fast neutron energy in the space environment. Through studies, the desired polymer was PEI (commercial name Ultem 1000) and the chosen neutron absorber was H_3BO_3. The experimental method was the solvent casting method using DMF solvent to dissolve PEI and H_3BO_3. The two constituents were mixed mechanically to achieve a homogeneous polymer composite. Another main objective of this thesis was to compare

the shielding effectiveness of the polymer composite based on their neutron absorber content (10 wt%, 20 wt% and 30 wt% H_3BO_3).

Unfortunately, due to the lack of time and experience, the material production did not provide the expected results. The thesis demanded a lot of knowledge and practical experience to achieve the best research outcome. The experimental process on the two constituents of the composite should have been tested many times to achieve the best outcome. With limited funding, not all aspects could be analysed to the fullest capacity. The production of PEI/H_3BO_3 composite could have been performed better by planning more carefully. The analysis of the experimental content of H_3BO_3 within the PEI matrix could have been studied and developed more using other methods than the UV-Vis technique. The neutron measurement should have taken place at least three times in a longer measuring time. Redoing all the experiments could provide more reliable results, if sufficient time was available. Furthermore, it is also proposed to test more aspects of material as a future task for assessing the overall suitability of the shielding composite in space performance. Generally, this thesis was still successful in proving the shielding potential of the PEI/H_3BO_3 composite against fast neutron energy that presents in the space environment. Although the experimental aim were not fully accomplished, the theory of using PEI/H_3BO_3 composite for neutron shielding in space condition (and even for nuclear application) is still possible for the future of space missions. Experimentally speaking, one would need to perform the proper experiments again at a longer time and carry out more characteristic studies to prove the theory.

REFERENCES

Abbasi, H., Antunes, M. & Velasco, J. I., 2015. Graphene nanoplatelets-reinforced polyetherimide foamsprepared by water vapor-induced phase separation. *eXPRESS Polymer Letters*, 9(5), pp. 412-423.

Angelis, A. D., 2013. Spontaneous Ionization to Subatomic Physics: Victor Hess to Peter Higgs. *Nuclear Physics B - Proceedings Supplements,* Volume 243–244, pp. 3-11.

Anon., 2009. *Sealed Radiation Sources,* Berlin: Eckert & Ziegler Nuclitec GmbH.

Anon., 2012. *Background document for N,N-Dimethylacetamide (DMAc).* [Online] Available at: https://www.echa.europa.eu/documents/10162/95105cf0-affb-4fd7-b9bb-c6923e793dd8
[Accessed 31 March 2020].

Anon., 2016. *Pulse-Height Spectrometry.* [Online] Available at: https://radiologykey.com/pulse-height-spectrometry/
[Accessed 12 April 2020].

Anon., 2017. *Charge Sensitive Preamplifier.* [Online] Available at: http://physicsopenlab.org/2017/09/27/charge-sensitive-preamplifier/
[Accessed 11 April 2020].

Anon., 2019. *Geiger–Müller tube.* [Online] Available at: https://en.wikipedia.org/wiki/Geiger%E2%80%93M%C3%BCller_tube
[Accessed 31 March 2020].

Anon., 2019. *What are Cosmic Rays?.* [Online] Available at: https://letstalkscience.ca/educational-resources/backgrounders/what-are-cosmic-rays
[Accessed 31 March 2020].

Anon., 2019. *What is space radiation?.* [Online] Available at: https://srag.jsc.nasa.gov/SpaceRadiation/What/What.cfm
[Accessed 21 January 2020].

Anon., n.d. *142IH Preamplifier.* [Online] Available at: https://www.ortec-online.com/products/electronics/preamplifiers/142ih [Accessed 11 April 2020].

Anon., n.d. *MCA-8000D Digital Multichannel Analyzer.* [Online] Available at: https://www.amptek.com/products/multichannel-analyzers/mca-8000d-digital-multichannel-analyzer
[Accessed 02 April 2020].

Anon., n.d. *Neutron Radioprotection.* [Online] Available at: https://www.radioactivity.eu.com/site/pages/Neutron_Radioprotection.htm [Accessed 31 March 2020].

Anon., n.d. *Proportional Counter – Proportional Detector.* [Online] Available at: https://www.nuclear-power.net/nuclear-engineering/radiation-detection/gaseous-ionization-detector/proportional-counter-proportional-detector/
[Accessed 02 April 2020].

Bate, N., 2009. *Monomer and Polyimide Production for Radiation Shielding Purposes in Manned Space Exploration,* Williamsburg: College of William and Mary.

Castley, D., Goodwin, C. & Liu, J., 2019. Computational and experimental comparison of boron carbide, gadolinium oxide, samarium oxide, and graphene platelets as additives for a neutron shield. *Radiation Physics and Chemistry,* Volume 165.

Cherry, R. N., n.d. *Chapter 48 - Radiation: Ionizing.* [Online] Available at: http://www.ilocis.org/documents/chpt48e.htm#:~:targetText=Directly%20ionizing%20radiation%20consists%20of,heavy%20ions%20(ionized%20atoms).&targetText=Indirectly%20ionizing%20radiation%20consists%20of%20uncharged%20particles.
[Accessed 16 November 2019].

Christesen, J., 2011. *Mechanical Pr Mechanical Properties of Solv ties of Solvent Cast Gr ent Cast Graphene-P aphene-Polymer,* Williamsburg: College of William and Mary.

Cleveland, R. F. & Ulcek, J. L., 1999. *Questions and Answers about Biological Effects and Potential Hazards of Radiofrequency Electromagnetic Fields,* Washington D.C: US Federal Communications Commission - Office of Engineering & Technology.

Collins, B. M., 2015. *Development of Boron-Containing Polyimide Materials and Development of Boron-Containing Polyimide Materials and Poly(arylene Ether)s for Radiation Shielding* , Stafford: College of William & Mar y - Arts & Sciences .

Connor, N., 2019. *What is Neutron Energy – Definition,* s.l.: Reactor Physics.

Daines, G., 2017. *NASA's Journey to Mars,* Washington D.C: National Aeronautics and Space Administration.

Daniel R. McAlister, 2016. *Neutron Shielding Materials,* Lisle: PG Research Foundation, Inc. 1955 University Lane Lisle, IL 60532, USA.

Eckhardt, R., 1995. Ionizing Radiation—It's Everywhere!. *Los Alamos Science,* Issue 22-24, p. 168.

El-Batanouny, M., 2020. *Advanced Quantum Condensed Matter Physics: One-Body, Many-Body, and Topological Perspectives.* Kindle ed. Cambridge: Cambridge University Press.

Fallon, A., 2012. *Hemoglob in Molecule and Spectroscopic Techniques used in determining Hemoglobin Concentration,* Dublin: Dublin City University.

Fisher, B. M. et al., 2011. *Fast Neutron Detection with 6Li-loaded Liquid Scintillator,* Laurel: s.n.

Friedberg, W. & Copeland, K., 2011. *Ionizing Radiation in Earth's Atmosphere and in Space Near Earth,* Oklahoma: Civil Aerospace Medical Institute - Federal Aviation Administration.

Guarino, F., Hauviller, C. & Tavlet, M., 2001. *Compliation of Radiation Damage Test Data*, Geneva: CERN.

H. Koshiishi, H. M. A. C. T. G. T. O., 2007. Evaluation of the neutron radiation environment inside the International Space Station based on the Bonner Ball Neutron Detector experiment. *Radiation Measurements,* Volume 42, pp. 1510-1520.

Hansen, C. M., 2007. *Hansen Solubility Parameters: A User's Handbook.* 2nd ed. Boca Raton: CRC Press.

Hawking, S., 2018. *BRIEF ANSWERS TO THE BIG QUESTIONS.* 1st ed. London: John Murray.

Herrman, K. et al., 2019. Mechanical characterization of polyethylene-based thermoplastic composite materials for radiation shielding. *Composites Communications,* Volume 13, pp. 37-41.

Imster, E. & Byrd, D., 2019. Today in science: Launch of Sputnik. *EarthSky,* 4 October.

J.Köhler, et al., 2015. Measurements of the neutron spectrum in transit to Mars on the Mars Science Laboratory. *Life Sciences in Space Research,* Volume 5, pp. 6-12.

Johnson, L. B., 2002. *Understanding Space Radiation,* s.l.: National Aeronautics and Space Administration.

Johnson, R. O. & Burlhis, H. S., 1983. Polyetherimide: A New High-Performance Thermoplastic Resin. *Journal of Polymer Science Polymer Symposia,* 70(1), pp. 129-143.

Jumpee, C. & Wongsawaeng, D., 2015. Innovative neutron shielding materials composed of natural rubber-styrene butadiene rubber blends, boron oxide and iron(III) oxide. *Journal of Physics: Conference Series,* Volume 611.

Kiefer, R. L., 2011. *Polymeric Materials with Additives for Durability and Radiation Shielding in Space,* Williamsburg: National Aeronautics and Space Administration.

Knoll, G. F., 2010. *Radiation Detection and Measurement,* Hoboken: John Wiley & Sons.

Landau, E., 2019. *Artemis Moon Program Advances – The Story So Far,* Washington D.C: National Aeronautics and Space Administration.

L'Annunziata, M. F., 2016. *Radioactivity: Introduction and History, From the Quantum to Quarks.* 2nd ed. s.l.:Elsevier.

Li, X. et al., 2018. High temperature resistant polyimide/boron carbide composites for neutron radiation shielding. *Composites Part B: Engineering,* Volume 159, pp. 355-361.

Lloyd, C. W., Pharm.D, Townsend, S. & Reeves, K. K., 2017. *Space Radiation.* Houston: NASA Human Research Program Engagement and Communications.

Logsdon, J. M., 2019. *Space Exploration.* [Online] Available at: https://www.britannica.com/science/space-exploration [Accessed 01 December 2019].

Marshal, G. C., 2007. What are Engineering Countermeasures?. In: *Radiation Countermeasures.* s.l.:Space Faring: The Radiation Challenge Unit - NASA, p. 4.

McMillan, J., 2019. *Radiation shielding composites using thermoplastic polymers mouldable at low temperature,* Sheffield: The University of Sheffield.

MERCK, 2009. *Material Safety Data Sheet for N,N-Dimethylformamide 110983.* [Online]
Available at: https://www.merckmillipore.com/FI/en/product/msds/MDA_CHEM-110983?Origin=PDP
[Accessed 11 December 2019].

Mills, K. C., 2010. *Solvent Manipulation, Dielectric Spectroscopy, and Rheological Analysis in the Electrospinning of a Rigid Rod Polymer,* New York: Faculty of the Graduate School of Cornell University.

Murray, R. L. & Holbert, K. E., 2019. Chapter 4 - Nuclear Processes. In: *Nuclear Energy.* 8th ed. Raleigh: Butterworth-Heinemann, pp. 53-79.

Nagavally, R. R., 2017. COMPOSITE MATERIALS - HISTORY, TYPES, FABRICATION TECHNIQUES, ADVANTAGES, AND APPLICATIONS. *International Journal of Mechanical And Production Engineering,* 5(9).

Nakamura, T., 2008. Cosmic-ray Neutron Spectrometry and Dosimetry. *Journal of Nuclear Science and Technology,* 45(sup5), pp. 1-7.

Nambiar, S. & Yeow, J. T. W., 2012. Polymer-Composite Materials for Radiation Protection. *ACS Applied Materials & Interfaces,* 4(11), pp. 5717-6402.

NASA, 2000. *Why we explore.* [Online] Available at: https://www.nasa.gov/exploration/whyweexplore/why_we_explore_main.html [Accessed 12 July 2019].

Özdemir, T., Akbay, I. K., Uzun, H. & Reyhancan, I. A., 2016. Neutron shielding of EPDM rubber with boric acid: Mechanical, thermal properties and neutron absorption tests. *Progress in Nuclear Energy,* Volume 89, pp. 102-109.

Özdemir, T., Güngör, A. & Reyhancan, İ., 2017. Flexible neutron shielding composite material of EPDM rubber with boron trioxide. *Radiation Physics and Chemistry,* Volume 131, pp. 7-12.

Paine, T. O., 1969. *APOLLO 11 (NASA SP-214) - Preliminary Science Report*, Washington DC: National Aeronautics and Space Administration .

Pavlenko, V. I., Cherkashina, N. I. & Yastrebinsky, R. N., 2019. Synthesis and radiation shielding properties of polyimide/bismuth-oxide composites. *Heliyon,* 5(5).

Perez, J., 2019. *Why Space Radiation Matters.* [Online] Available at: https://www.nasa.gov/analogs/nsrl/why-space-radiation-matters [Accessed 21 January 2020].

Rajasekar, S. & Venkatesan, D., 2012. Synthesis and Properties of Polyetherimides by Nucleophilic Displacement Reaction. *Polymers & Polymer Composites,* 20(9), pp. 845-852.

Reine, A. H., Hinojosa, O. & Arthur, J. C., 2003. Effects of dipolar aprotic solvents on the stability of free radicals in γ-irradiated cotton cellulose. *Journal of Polymer Science Part B: Polymer Letters,* 9(7), pp. 503-507.

Révay, Z., Lindstrom, R. M., Mackey, E. A. & Belgya, T., 2011. Neutron-induced Prompt Gamma Activation Analysis (PGGAA). In: A. Vértes, et al. eds. *Handbook of Nuclear Chemistry.* s.l.:Springer, pp. 1619-1673.

Rogers, K., 2009. Ionizing Radiation Injury. *Britannica Academic,* 06 February.

Satterfield, D., 2009. How Much Radiation Does it Take to Kill You?. *Dan's Wild Wild Science Journal.*

Scarlet, R. et al., 2012. Study on the solubility of polyetherimide for nanostructural electrospinning. *Revista de Chimie,* 63(7), pp. 688-692.

Selph, W. et al., 1968. Neutron Attenuation. In: R. G. Jaeger, et al. eds. *Engineering Compendium on Radiation Shielding.* Heidelberg: Springer-Verlag Berlin Heidelberg, pp. 259-362.

Shin, J. W. et al., 2014. Polyethylene/boron-containing composites for radiation shielding. *Thermochimica Acta,* Volume 585, p. 5–9.

Siemann, U., 2005. Solvent cast technology – a versatile tool for thin film production. In: N. Stribeck & B. Smarsly, eds. *Scattering Methods and the Properties of Polymer Materials.* Weil am Rhein: Springer, Berlin, Heidelberg, pp. 1-14.

Singh, L., 2017. Who Discovered the Neutron?. *Who Invented*, 20 September, p. 1.

Soltani, Z., Beigzadeh, A., Ziaie, F. & Asadi, E., 2016. Effect ofparticle size and percentages of Boron carbide on the thermal neutron radiation shielding properties of HDPE/B4C composite:Experimental and simulation studies. *Radiation Physics and Chemistry,* Volume 127, p. 182–187.

Soltani, Z., Beigzadeh, A., Ziaie, F. & EskandarAsadi, 2016. Effect of particle size and percentages of Boron carbide on the thermal neutron radiation shielding properties of HDPE/B4C composite: Experimental and simulation studies. *Radiation Physics and Chemistry,* Volume 127, pp. 182-187.

Tanaka, T. et al., 2019. Gamma Ray Spectra from Thermal Neutron Capture on Gadolinium-155 and Natural Gadolinium. *Progress of Theoretical and Experimental Physics (PTEP),* pp. 3-14.

Thibeault, S. A. et al., 2012. *Radiation Shielding Materials Containing Hydrogen, Boron, and Nitrogen: Systematic Computational and Experimental Study - Phase I,* Hampton: NASA Institute for Advanced Concepts.

Vora, R. H., Sawant, P. D., Goh, S. H. & Vora, M., 2005. Fluoro-poly(ether imide)s and fluoro-poly(ether imide)/organa-soluble MMT clay nanocomposites: Synthesis, fabrication, characterization and thermal degradation kinetics study of their films. In: K. L. Mittal, ed. *Polyimides and Other High Temperature Polymers: Synthesis, Characterization and Applications.* London: CRC Press, pp. 201-265.

Wikipedia contributors, 2019. *Cosmic ray*. [Online] Available at: https://en.wikipedia.org/wiki/Cosmic_ray [Accessed 10 September 2019].

Williams, M., 2017. What is Low Earth Orbit?. *Universe Today - Space and Astronomy news*, 06 Juanuary.

Worsfold, P. J. & Zagatto, E. A. G., 2019. Spectrophotometry | Overview. In: P. Worsfold, A. Townshend, C. Poole & M. Miró, eds. *Encyclopedia of Analytical Science.* s.l.:Elsevier Science and Technology, pp. 244-248.